DEPARTMENT OF OCEAN ENGINEERING

MASSACHUSETTS INSTITUTE OF TECHNOLOGY

CAMBRIDGE, MASSACHUSETTS 02139

DEVELOPMENT OF A FLOATING ELEMENT

WALL SHEAR TRANSDUCER

STEVEN WALTER PETRI

S.M., M.E.
O.E.

13-A
JUNE 1984

N66314-70-A-0073

DEVELOPMENT OF A FLOATING ELEMENT WALL SHEAR TRANSDUCER

by

STEVEN WALTER PETRI

B.S., United States Naval Academy
(1978)

Submitted to the Department of
Ocean Engineering
in Partial Fulfillment of the
Requirements of the Degrees of

OCEAN ENGINEER

and

MASTER OF SCIENCE IN MECHANICAL ENGINEERING

at the

MASSACHUSETTS INSTITUTE OF TECHNOLOGY

June 1984

Signature of Author: Steven Walter Petri
Department of Ocean Engineering, 11 May 1984

Certified by: Patrick Leehey
Thesis Supervisor

Accepted by: A. Douglas Carmichael
Chairman, Ocean Engineering Departmental Committee

Accepted by: Warren M. Rohsenow
Chairman, Mechanical Engineering Departmental Committee

DEVELOPMENT OF A FLOATING ELEMENT WALL SHEAR TRANSDUCER

by

STEVEN WALTER PETRI

Submitted to the Department of Ocean Engineering
on 11 May 1984 in partial fulfillment of the
requirements for the degrees of Ocean Engineer and
Master of Science in Mechanical Engineering

ABSTRACT

A highly linear passive floating element wall shear transducer has been developed which uses a sensitive frequency modulation technique to measure a capacitance change proportional to the displacement of the floating element for small deflections. The floating element is 4 mm square surrounded by a gap nominally 0.18 mm and protrudes into the boundary layer 9 μm. Scaled on inner parameters, each side of the sensing head measures about 290, the mean gap width is 13, and the element protrusion is 0.7. The transducer was tested in a turbulent boundary layer on a flat plate at momentum thickness Reynolds numbers of 3140, 3500, and 3760 and the results compared to wall shear stress estimates obtained from the law of the wall. The transducer was found to predict the steady mean wall shear stress within the limits of experimental uncertainty in all cases; transducer measurements of mean wall shear stress for momentum thickness Reynolds numbers of 3140 and 3500 were within 2 percent of the actual value. Transducer measurement of the unsteady mean wall shear stress was severely limited by a mechanical resonance in the transducer at 63 Hz.

The operating principles and general characteristics of the transducer are discussed, its performance is evaluated, and recommendations are made concerning future work.

Thesis Supervisor: Dr. Patrick Leehey

Title: Professor of Applied Mechanics

per Form 50 on file.

A-1

ACKNOWLEDGEMENTS

I would like to thank all those who have helped me in this research. Discussions with other students in the Acoustics and Vibration Laboratory have been invaluable, as was their assistance in getting things done. Special thanks to my office partner Tom Korsmeyer who was a ready and willing sounding board and whose advice was timely and priceless. Russ McDonnell of MIT's Microelectronics Laboratory was also a big help; he opened my eyes to the capabilities of microelectronics. I am particularly indebted to Professor Patrick Leehey who made all this work possible; I deeply appreciate his patience during the last weeks of this research. Finally, thanks to my wife Debbie for her love when my mind was elsewhere and her assistance when the schedule got hectic.

This research was supported in part under Office of Naval Research contract N00014-78-C0696.

TABLE OF CONTENTS

APPENDICES

LIST OF FIGURES

LIST OF TABLES

NOMENCLATURE

A_e surface area of the floating element;

C capacitance of the cantilever-stationary plate pair

C_f friction coefficient

d_o mean spacing between stationary and cantilever plates with the cantilever undeflected

e_ζ uncertainty or error in the quantity ζ

EI the flexural rigidity of the cantilever beam

F generally, a force; in Appendix C, a functional expression for the quantity being measured

f frequency in Hz; in Appendix A, a force distributed the length of the beam element $(f(x,t))$

f_o center frequency of astable multivibrator

f_1 fundamental mechanical resonant frequency of the beam element

G gain in the frequency-to-voltage converter and instrumentation amplifier, V/Hz

J mass moment of inertia of the floating element

k surface roughness

k_s static spring constant of cantilever beam to transverse loads, $3EI/L^3$

L length of the cantilever plate and beam element

M mass of the floating element (assumed to be a point mass)

m mass of the beam

q the total head, $\frac{1}{2}\rho U_\infty^2$; also the total error (Appendix C)

R electrical resistance

Re_x Reynolds number based on x, the distance from the plate's leading edge

Re_θ momentum thickness Reynolds number

s sensitivity of the transducer in either V/Pa or V/μm; also the spacing between capacitor plates (Appendix A)

t thickness of the cantilever plate ; also time

u longitudinal fluctuating fluid velocity

U_∞ free stream velocity

U_τ friction velocity, $\sqrt{\frac{\tau_w}{\rho}}$

V_o transducer offset voltage

$V(t)$ transducer output voltage

w width of the cantilever plate; also (Appendix A) the weight per unit length of the beam

W weight of the floating element

x referring to the flow, the streamwise distance from the plate's leading edge; referring to the beam element, the distance along the beam from the base of the beam

y referring to the flow, the distance normal to the wall measured from the wall; referring to the beam element, the deflection of the beam element from its undeflected position

z the deflection of the beam with respect to a stationary observer

δ boundary layer thickness; also (Appendix A) the variational operator used in the variational calculus

δ^* displacement thickness

ε transverse deflection of the free end of the cantilever; also the percent most probable error (Appendix C)

λ^* the viscous length scale, $\frac{\nu}{U_\tau}$

η beam deflection normalized on mean capacitor spacing d_o

ξ normalized coordinate along beam, x/L

θ momentum thickness

θ_o transducer inclination angle from the vertical

ϕ floating element angle of rotation

$\bar{\tau}_w$ wall shear stress; mean wall shear stress refers to a spatial average as opposed to steady wall shear stress which implies a time average

ν kinematic viscosity

Superscripts

+ identifies the quantity as being nondimensionalized in inner coordinates; velocities are normalized on U_τ and lengths are normalized on λ^*

Subscripts

∞ refers to free stream properties

w refers to quantities measured at the wall

1. INTRODUCTION

1.1 BACKGROUND

For many centuries, men have studied the force of drag which resists the motion of a body through a fluid. Todd (1967) reports that as early as the late fifteenth century, Leonardo da Vinci conducted tests on three ship models with different hull forms, presumably to identify the most efficient design.

The dawn of the "age of steam" in the late nineteenth century motivated researchers to better understand fluid drag in order to both predict and minimize its effect. As sailing ships were supplanted by larger and faster self-propelled ships, friction drag was recognized as a sizeable contributor to the overall fluid drag. William Froude (1872) conducted a series of friction drag measurements in his towing tank at Torquay, England, to analyze the effect of friction drag on ships. Froude built planes from wooden planks and towed them edge-first through the water, measuring their drag with a dynamometer. In so doing, Froude actually determined the mean wall shear stress acting over the surface of each plane.

Since 1904, when Prandtl presented his boundary layer theory to the Mathematical Congress in Heidelberg, understanding of the

wall shear stress has grown considerably in sophistication. While Froude intuitively grasped that the distribution of wall shear stress over a body in a fluid flow was not uniform, theory now predicts that the wall shear stress is a function of both space and time. This dynamic, nonhomogeneous nature of the wall shear stress is particularly evident in the transition and turbulent regions of the boundary layer.

The wall shear stress is also an important boundary layer parameter in its own right since it is a characteristic of the inner region of the boundary layer (near the wall) where viscous forces predominate. Many researchers have found that boundary layer processes scale on the wall shear stress, particularly those related to turbulence in the transition and fully turbulent regions of the boundary layer. One example is the familiar "law of the wall" in which the turbulent mean velocity profile is nondimensionalized on mean wall shear stress and kinematic viscosity [see Coles (1968) and White (1974)]. Burton (1974) found that turbulent wall pressure spectra and corresponding fluctuating longitudinal velocity spectra scaled on the wall shear stress. Gedney (1979) was unable to collapse his transition wall pressure spectra because of inaccurate determination of the wall shear stress upon which they were nondimensionalized. In short, ongoing fundamental boundary layer research indicates that more precise measures of the wall shear stress than currently available are increasingly necessary.

1.2 WALL SHEAR STRESS

Wall shear stress, like any stress, is a derived quantity and thus cannot be measured directly. The wall shear stress is a dynamic quantity defined at a point by the following limit:

$$\tau_w \equiv \lim_{A \to 0} \frac{F}{A} \tag{1.1}$$

where F is the friction force acting over area A. Unless the measurement of the wall shear force is made at a single point, the best we can expect to measure is a mean wall shear stress averaged over some measurement area. Measurement techniques used to determine wall shear stress are, in reality, merely techniques which measure quantities related to the wall shear stress from which the wall shear stress is inferred. As the measurement area approaches a point, the measured wall shear stress approaches the true wall shear stress according to equation 1.1. Small measurement areas thus strengthen the inference that the measured shear stress is the true shear stress, underscoring the need for good spatial resolution if the true shear stress at a point is the subject of investigation.

1.3 MEASUREMENT TECHNIQUES

Table I, adapted from Winter (1977), provides a brief listing of the mean wall shear stress measurement techniques currently in use. No single technique is universally acceptable because each has restrictions on its application to different flow conditions and possesses limited versatility. Further, no technique can make an adequate measure of the true wall shear stress, owing to excessive spatial averaging or inadequate bandwidth. The hot film probe, using the heat transfer analogy, is the only device with sufficient bandwidth to measure some of the unsteady character of the mean wall shear stress. However, its spatial resolution and sensitivity are both poor.

TABLE I
Mean Wall Shear Stress Measurement Techniques

Analogies	Flow About Obstacles
Heat Transfer	Preston Tubes
Mass Transfer	Stanton Tubes
	Razor Blades
	Steps & Fences
Liquid Films	Static Pressure Holes
Floating Element	Momentum Balance
Velocity Profiles (Wall Similarity)	

In an effort to improve the resolution of dynamic wall shear stress measurements, a new type of floating element transducer has been developed and tested. This device uses a capacitance-measuring technique of exceptional sensitivity [first developed by Moeller (1983)] to measure the deflection of a small floating element in the plane of the wall. The sensitivity of the transducer permits its operation with such small motions of the floating element that the device exhibits excellent linearity. Thus, the powerful techniques of linear systems analysis may be used to uniquely and simply relate statistics of the transducer output to corresponding statistics of the mean wall shear stress.

2. TRANSDUCER DESIGN

2.1 GENERAL DESCRIPTION

The transducer is a passive floating element instrument which generates a voltage proportional to the displacement of the element and, indirectly, to the shear force acting on the element. This is unlike most floating element devices, which generally employ an active force-balance principle so that the element remains nearly stationary. The work of Kistler [Paros, (1970)], Allen (1980), Frei and Thomann (1980), Escudier, et. al. (1982), and Nguyen, Dickenson, et. al. (1984) are all examples of the active technique. In the current design, sensitivity has been improved to the point that the floating element deflects less than 5 μm. For a streamwise deflection of 5 μm, the floating element protrudes only 0.63 μm into the boundary layer, which is a y^+ of 5×10^{-2}. The protrusion due to floating element deflection is thus well within the viscous sublayer and can be neglected.

Figure 2.1 presents a schematic of the transducer. The beam element is the moving element of the transducer, composed of the floating element and a thin cantilever plate. The floating element, mounted in the plane of the wall atop the cantilever plate, is sensitive to motion in only one direction. Shear forces on

the surface of the element in the sensitive direction deflect the cantilever plate, producing a change in capacitance with respect to a second plate parallel to and mounted a short distance from the cantilever plate. This change in capacitance, proportional to floating element deflection for small displacements, changes the frequency of a square-wave oscillator. The transducer thus produces a frequency-modulated signal proportional to the floating element displacement which is subsequently demodulated and filtered by signal conditioning electronics.

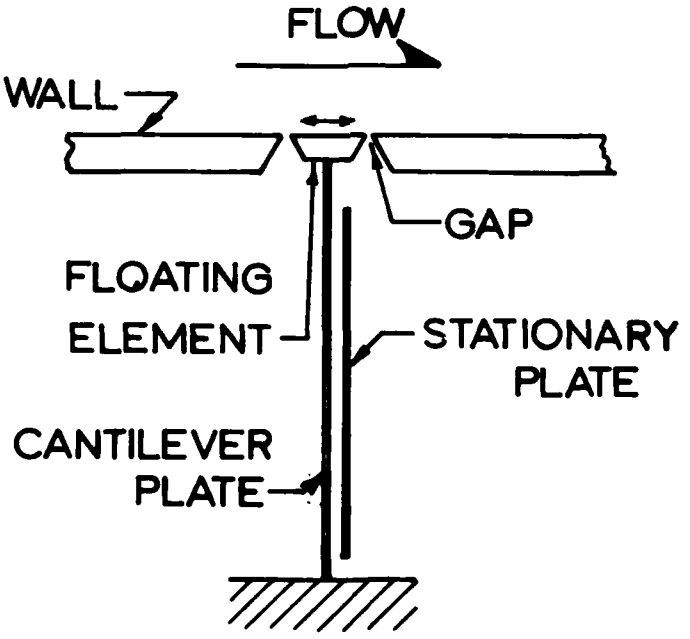

FIGURE 2.1 Transducer Schematic - General

2.1.1 Transducer Mechanical

The transducer is assembled within a body of phenolic-impregnated linen as shown in Figure 2.2. A shallow slot, milled in the body halves before assembly, contains a stationary capacitor plate of copper-clad laminate epoxied in place.

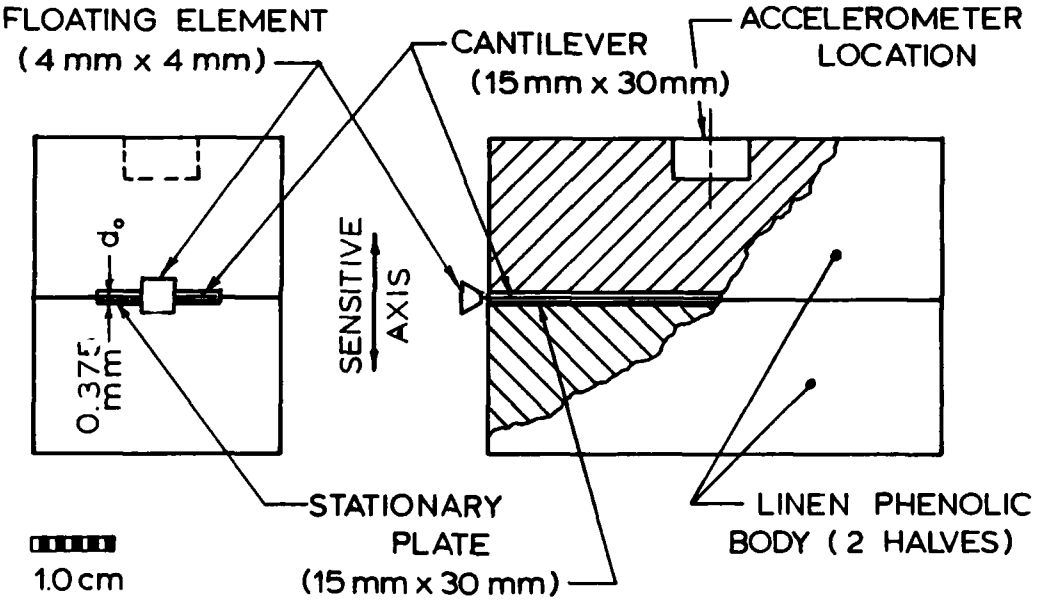

FIGURE 2.2 Transducer Schematic

The movable capacitor plate, made from 0.005 inch (0.13 mm) thick sheet brass shim stock, is sandwiched between the halves of the transducer body which are epoxied and screwed together. A floating element 4 mm square is cast in place atop the cantilever

plate using an epoxy potting compound. The square shape of the floating element was selected to minimize the degradation in transducer sensitivity caused by sealing the gap around the element.

The transducer is then mated to an aluminum adapter machined to accomodate the test fixture as indicated in Figure 2.3. An aluminum cylinder also mates with the adapter, shielding the transducer and its electronics from electromagnetic interference. Brass shims between the transducer and the adapter are used to position the floating element parallel to the top of the adapter with the top of the floating element protruding less than 0.1 mm from the surface of the adapter. The tops of the adapter and floating element, spray painted with flat white enamel before assembly, were lightly sanded with fine wet sandpaper to reduce the misalignment of the floating element with the wall to 9 μm. By sanding perpendicular to the transducer's sensitive direction, motion of the floating element and curvature of its upper surface were minimized. The gap around the element is not symmetric, ranging from 0.1 mm to 0.25 mm with a mean of 0.18 mm. An accelerometer mount is provided on the side of the transducer assembly inside the cylinder in order to monitor the acceleration of the transducer in its sensitive direction.

Table II summarizes the key lengths of the floating element in both dimensional form and in inner coordinates, nondimension-

alized on the viscous length λ^* characteristic of the boundary layer in which the transducer was ultimately tested.

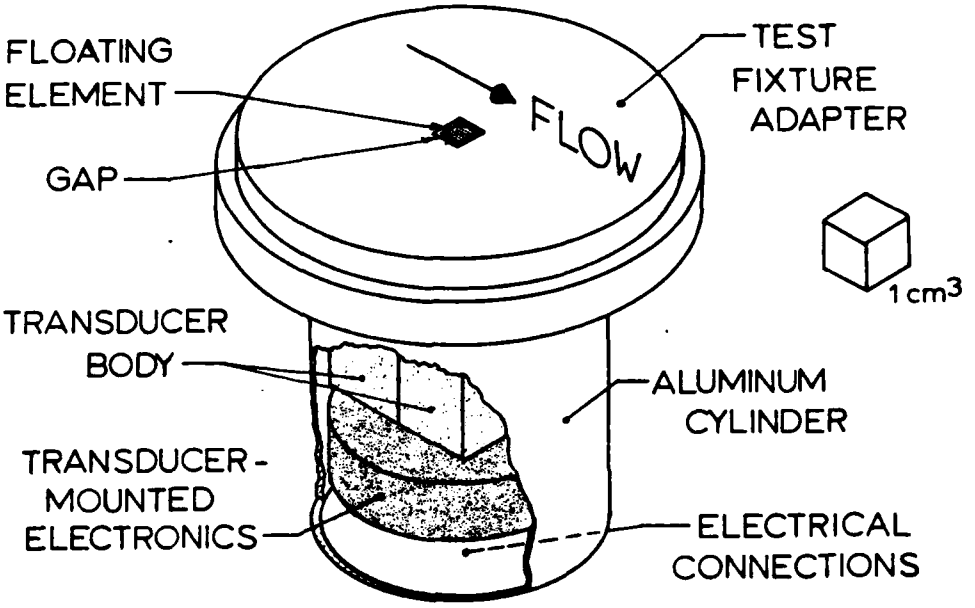

FIGURE 2.3 Transducer - Pictorial

TABLE II
Floating Element Dimensions

Dimension		ζ	ζ^+
gap	max.	0.25 mm	18
	min.	0.10 mm	7
	mean	0.18 mm	13
Protrusion		9 μm	0.69
Element Size		4 mm	290

ζ^+ is based on the experimental result U_τ = 1.3 m/s at U_∞ = 30.5 m/s.

2.1.2 Transducer Electronics

The electronics associated with the transducer fall into two categories: electronics physically mounted beneath the phenolic transducer assembly, and signal conditioning electronics installed in a separate enclosure. Each set of electronics uses shielded precision power supplies (Analog Devices model 904) which are bypassed to ground through 1.0 μF electrolytic capacitors. Further, each integrated circuit power supply pin is bypassed to ground through a 0.1 μF ceramic capacitor.

Figure 2.4 highlights the significant features of the electronic circuitry.

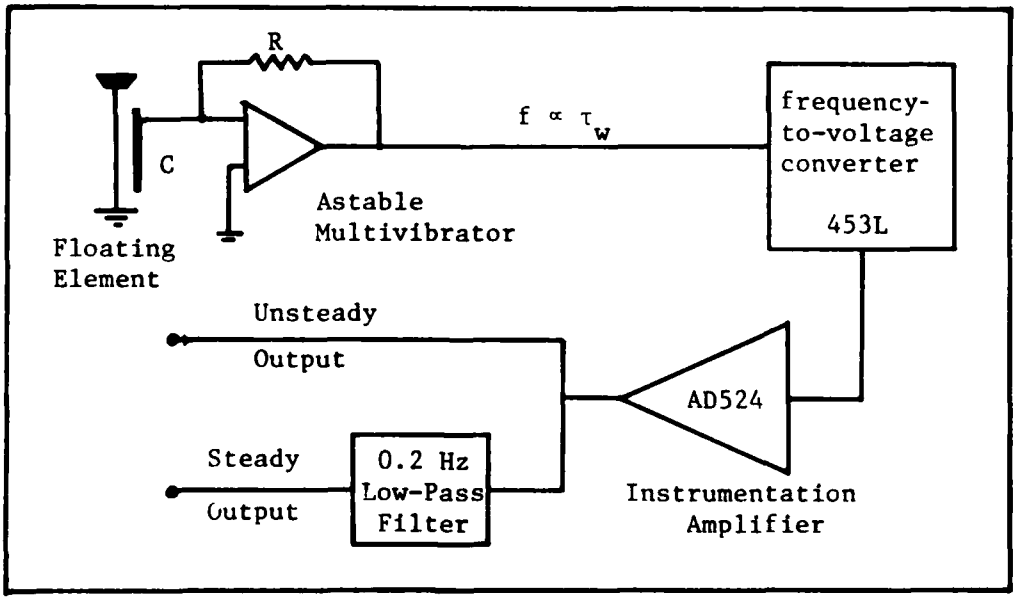

FIGURE 2.4 Circuitry - Block Diagram

Transducer-mounted electronics consist of the frequency modulator and a buffer amplifier. The frequency modulator is an astable multivibrator which produces a square wave nominally 6.2 V in amplitude at a frequency determined by the variable capacitor formed by the fixed and cantilever plates. When the cantilever plate is undeflected, the capacitance measures about 30 pF and the oscillator's frequency is about 55.6 kHz. An LM310 voltage follower is used as an isolation amplifier that drives a shielded BNC transmission line to the signal conditioning electronics. Power is supplied to the transducer-mounted electronics through a shielded cable from a power supply in a separate enclosure. The multivibrator circuit is taken from Jung (1980).

The signal conditioning electronics are mounted in a shielded aluminum box containing an integral power supply. An Analog Devices 453L precision frequency-to-voltage converter demodulates the transducer's frequency modulated signal, converting it to a voltage that is proportional to the received frequency. Both the gain and the offset of the frequency-to-voltage conversion are adjustable for calibration. An AD524 instrumentation amplifier (with selectable gains of 1, 10, 100, or 1000) amplifies the demodulated signal and drives both an active filter and a transmission line for measuring the fluctuating signal. The active filter, taken from Lancaster (1982), is a first-order low pass filter with cutoff frequency of 0.2 Hz. The filter drives a separate line for measuring the steady transducer output.

2.2 TRANSDUCER RESPONSE CHARACTERISTICS

It is shown in Appendix A.3 that the response of the transducer is described by the following equation in the limit of small deflections of the floating element:

$$V(t) = V_o + \frac{3 A_e G f_o}{8 k_s d_o} \bar{\tau}_w(t) \qquad (2.1)$$

where

- $\bar{\tau}_w(t)$ = the mean wall shear stress acting on the floating element;
- $V(t)$ = the output voltage from the signal conditioning electronics;
- A_e = the surface area of the floating element exposed to the flow;
- d_o = the mean separation between the undeflected capacitor plates;
- f_o = the oscillator center frequency;
- G = the total gain in the frequency-to-voltage converter and the instrumentation amplifier;
- k_s = the transverse stiffness of the cantilever beam when statically loaded at its free end; and
- V_o = the offset voltage.

Equation 2.1 is applicable for small displacements of the float-

ing element and for frequencies much smaller than the first resonant frequency of the beam element.

Equation 2.1 may be rewritten as

$$V(t) = V_o + s_\tau \bar{\tau}_w(t) \quad , \tag{2.2}$$

where

$$s_\tau \equiv \frac{\partial V}{\partial \tau_w} = \frac{3 A_e G f_o}{8 k_s d_o} = 0.40 \text{ V/Pa} \tag{2.3}$$

is the transducer's sensitivity. A related sensitivity is the transducer output per micron of floating element deflection

$$s_\varepsilon \equiv \frac{k_s}{A_e} s_\tau = \frac{3 G f_o}{8 d_o} = 0.56 \text{ V/}\mu\text{m} \quad . \tag{2.4}$$

The limits of the validity of equation 2.1 may be investigated by using the predicted beam element deflection shape determined in Appendix A.3 to evaluate the theoretical transducer output. From the appendix,

$$\frac{V(t) - V_o}{G f_o} = \frac{1}{\int_0^1 \frac{d\xi}{1 + \eta(\xi,t)}} - 1 \tag{2.5}$$
$$\text{(A1.15)}$$

and

$$\eta(\xi,t) = \frac{\varepsilon}{2d_o}(3\xi^2 - \xi^3) , \qquad (2.6)$$
$$(A3.4)$$

where $\frac{V(t) - V_o}{G\, f_o}$ is the normalized transducer output and $\eta(\xi,t)$ is the deflection shape of the beam element normalized on d_o. Equation 2.6 describes the static deflection shape of the beam element for a force applied to the floating element and is valid for frequencies much smaller than the fundamental mechanical resonance. The integral in equation 2.5 may be performed numerically using equation 2.6 and the normalized transducer output plotted as a function of the normalized end deflection of the beam $\frac{\varepsilon}{d_o}$. As shown in Figure 2.5, the transducer is linear to within 1.25 percent proportional error up to $\left|\frac{\varepsilon}{d_o}\right| = 0.05$. Given that $k_s = 22.5$ N/m, $A_e = 16$ mm^2, and $d_o \simeq 375$ μm, the device is effectively linear up to $\left|\overline{\tau}_w\right| = 26$ Pa since

$$\left|\overline{\tau}_w\right|_{max} = \frac{k_s}{A_e}\left|\varepsilon\right|_{max} = \frac{k_s\, d_o}{A_e}\left|\frac{\varepsilon}{d_o}\right|_{max} \qquad (2.7)$$

For the turbulent boundary layers considered in the current research, $\left|\overline{\tau}_w\right|_{max} \simeq 5$ Pa so that the normal operating regime is the much smaller box shown in Figure 2.5.

The natural frequencies of the transducer response are obtained in Appendix B by evaluating the eigenvalues of the beam element's free vibration response. For the first two vibration modes of the beam element, the rotational inertia of the floating

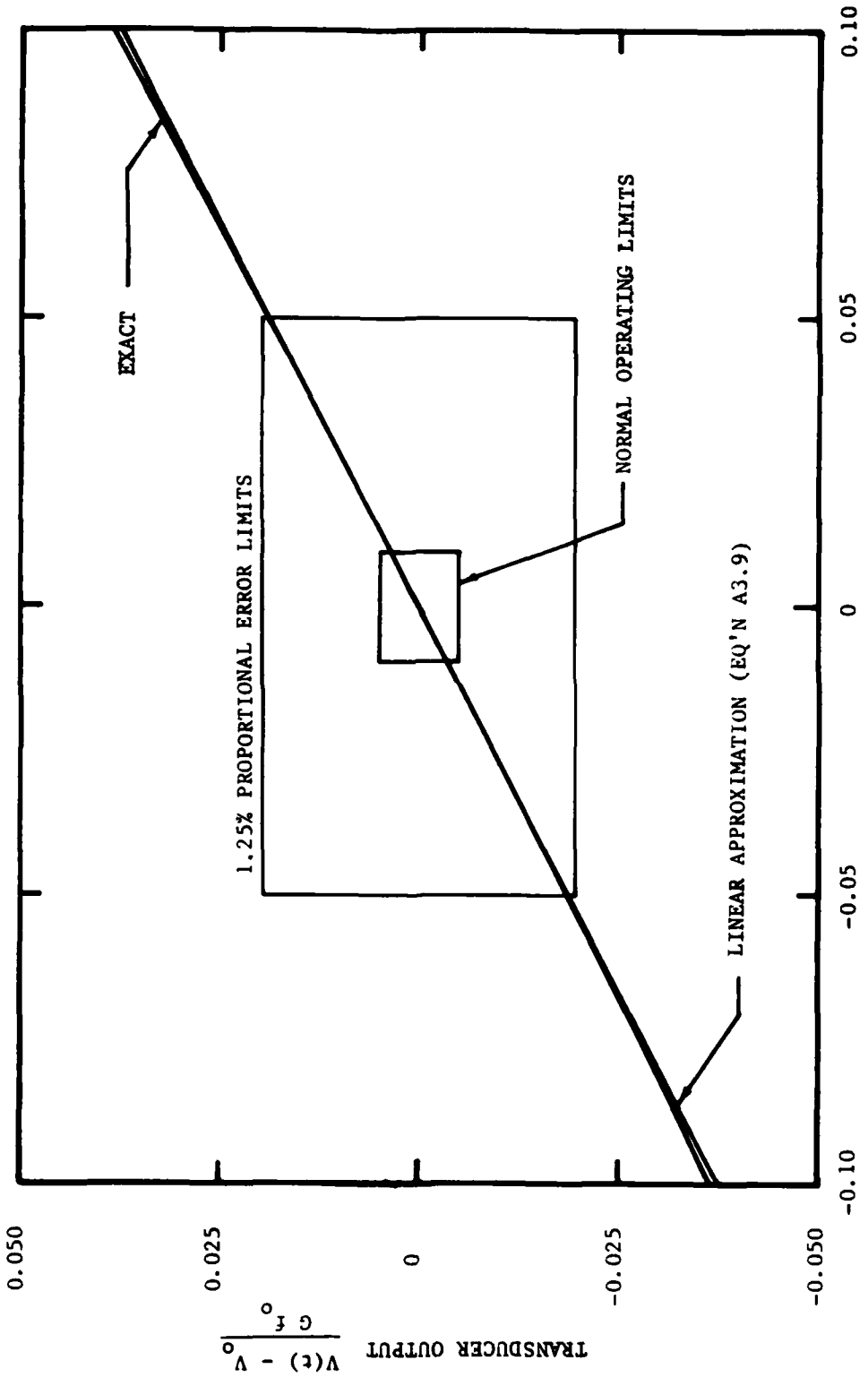

FIGURE 2.5 Transducer Linearity

element was calculated to affect the natural frequencies by less than 1.0 percent and so was neglected. Calculation of the transducer's natural frequencies is complicated by an ambiguity in the beam length introduced by the spatial extent of the floating element. Contrary to the model, the floating element is not a point mass but rather extends over 6 percent of the cantilever plate's length. The fundamental resonant frequency of the beam element is estimated from the model to be 61.7 Hz, with an uncertainty of 6.3 percent. Measurements of the dynamic characteristics of the transducer presented in greater detail in section 4.1 indicate that the fundamental resonance is actually 63 Hz.

Characteristics of the transducer are summarized in Table III.

TABLE III
Transducer Characteristics

Mass:	Floating Element	76 mg
	Cantilever Plate	480 mg
		≈ 16 g/m
Stiffness:		22.5 N/m
Fundamental Resonance:		63 Hz
Sensitivity:	s_τ	= 0.40 V/Pa
	s_ε	= 0.56 V/μm end deflection
Spatial Resolution:		4 mm x 4 mm

Inclination of the transducer from the vertical in a gravity field generates a response from the transducer, since then a component of the weight of the beam element is transverse to the beam. The transducer exhibits buckling behavior when inclined, because the transverse force tends to increase the deflection of the beam and itself increases as the local inclination angle of the beam increases. Transducer inclination response is analyzed in Appendix A.4 in the limit of small static inclinations of the transducer base. The expression obtained in the appendix for the deflection of the beam element $\eta(\xi,t)$ with inclination angle θ_o (equation A4.7) is then inserted in equation 2.5, which is in turn integrated numerically to obtain the transducer output as a function of inclination angle plotted in Figure 2.6.

The theoretical response of the transducer to inclination is sensitive to the beam length L and mean capacitor spacing d_o, as indicated in Figure 2.6 by comparing the solid and dashed lines. The solid line is the theoretical transducer response for the beam length and mean capacitor spacing used in all calculations; the dashed line is the theoretical response for a beam length 1 mm (3.2%) smaller and mean capacitor spacing 25 μm (6.7%) larger. The variations in the parameters used to generate the dashed line are representative of uncertainties in those parameters due to manufacturing limitations.

A simple experiment was conducted to verify the theoretical

response predicted in Figure 2.6. Experimental results are also plotted in Figure 2.6 and may be seen to lie within the limits of uncertainty in predicted response. Also indicated on the figure are the expected operating limits of the transducer in the current research from Figure 2.5, corresponding to $\left|\bar{\tau}_w\right|$ = 5.0 Pa at zero inclination angle. The transducer output due solely to rotation of the transducer base one degree from the vertical is of the same order as the transducer output due solely to wall shear stress, indicating the importance of maintaining the attitude of the transducer.

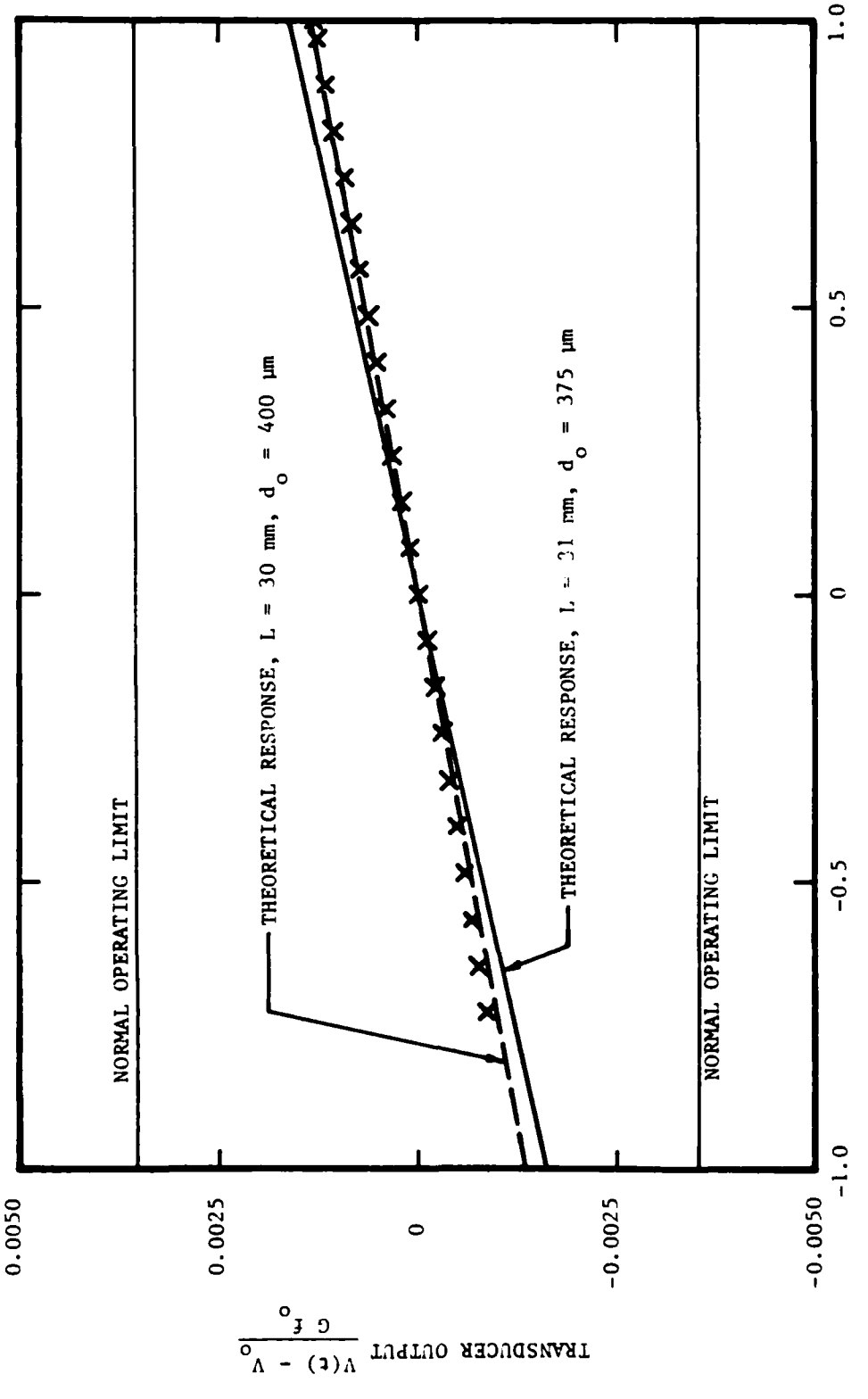

FIGURE 2.6 Transducer Response to Inclination

3. EXPERIMENTAL EQUIPMENT AND INSTRUMENTATION

3.1 EXPERIMENTAL FACILITY

The transducer was tested in the MIT low-noise, low-turbulence open circuit wind tunnel. This facility is shown in Figure 3.1 and is described in detail by Hanson (1969). It has a flow speed range of 20 to 50 m/s, controlled by varying the speed of a DC motor driving the blower. The array of turbulence reducing screens between the honeycomb flow straightener and the settling zone maintains the free stream turbulence level less than approximately 0.05%. A test section 38 cm (15 inches) square and 183 cm (6 feet) long was mounted in an open jet configuration within the airtight blockhouse immediately behind the contraction. The test section, lined with smooth sound absorptive material, has movable walls for controlling the longitudinal pressure gradient. A mechanical x-y traverse accurate to 0.025 mm (0.001 inch) vertically and to 2.5 mm (0.1 inch) horizontally is installed on the test section and used to position a hot wire or a pressure probe during the measurement of mean flow properties in the test section.

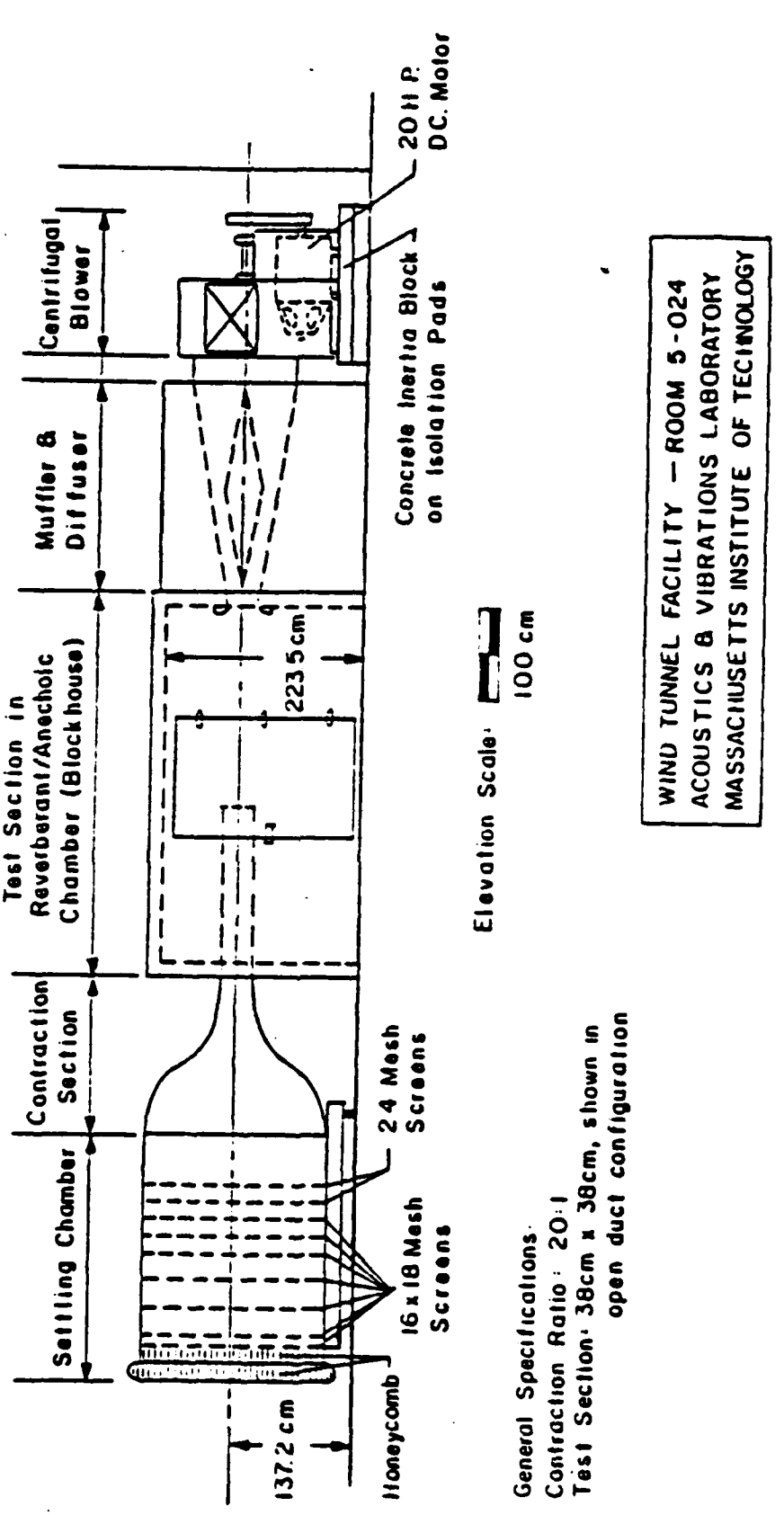

FIGURE 3.1 Test Facility

3.2 TEST FIXTURE

The test fixture is a damped aluminium flat plate described in detail by Gedney (1979), who used it while investigating transition region wall pressure fluctuations. The plate, sketched in Figure 3.2, is 38 cm (15 inches) wide and 122 cm (48 inches) long; the upper surface is polished to a 0.1 micron root mean square (rms) surface roughness. The plate's leading edge is a solid tool and jig plate, 1.27 cm (0.50 inch) thick, machined into a 6:1 ellipse. The test plate's trailing edge consists of a thin splitter plate which extends rearward to prevent coherent vortex shedding from creating plate vibrations.

The test plate was mounted horizontally in the test section 13 cm (5 inches) above the bottom to minimize secondary flow effects observed by Shapiro (1977). The walls of the test section were then adjusted to provide a minimum pressure gradient. The variation in pressure obtained over the length of the plate at a free stream velocity of 35 m/s is shown in Figure 3.3. The maximum variation observed (excluding the leading edge) was less than 2% of the total head. The transducer was installed at the location indicated.

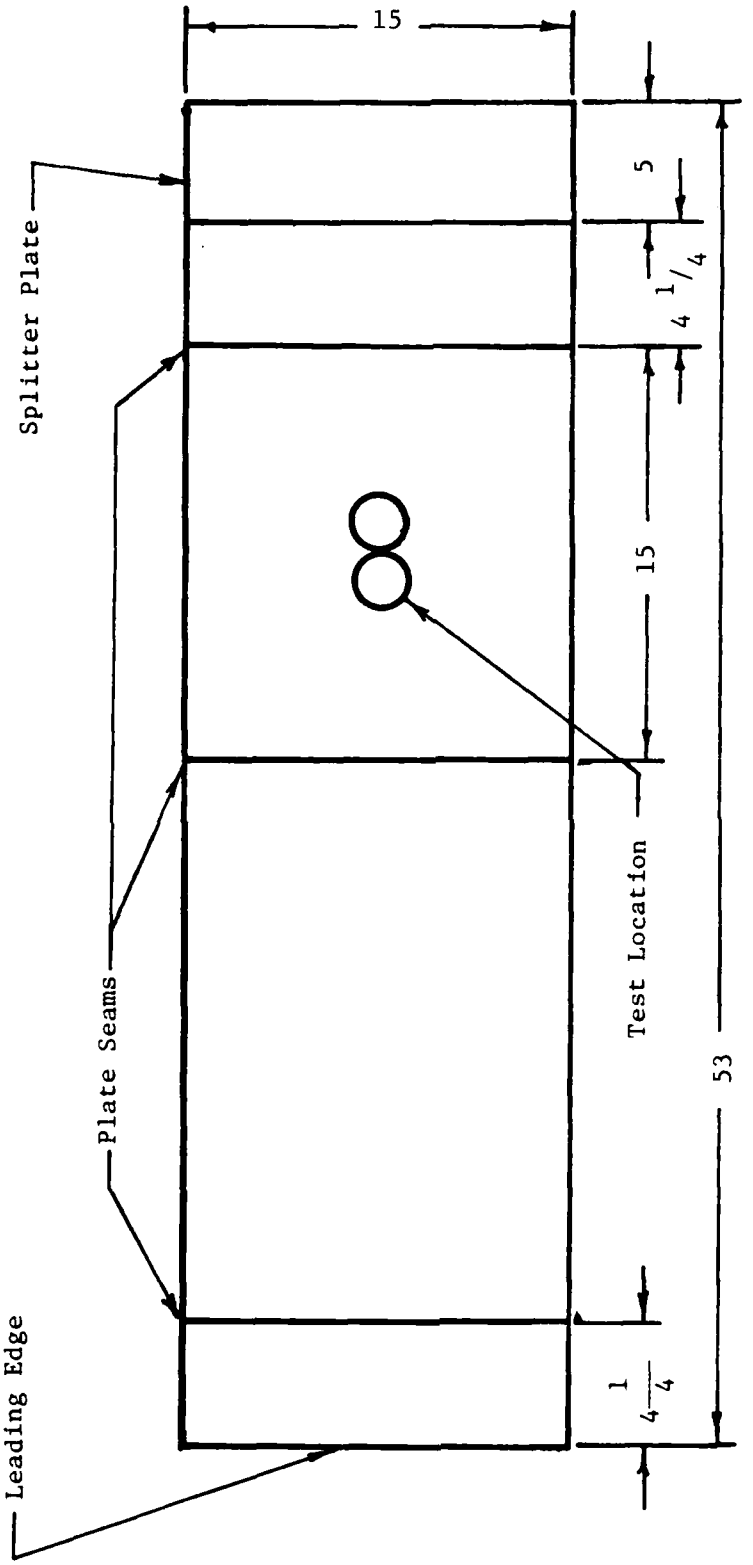

FIGURE 3.2 Test Plate Layout

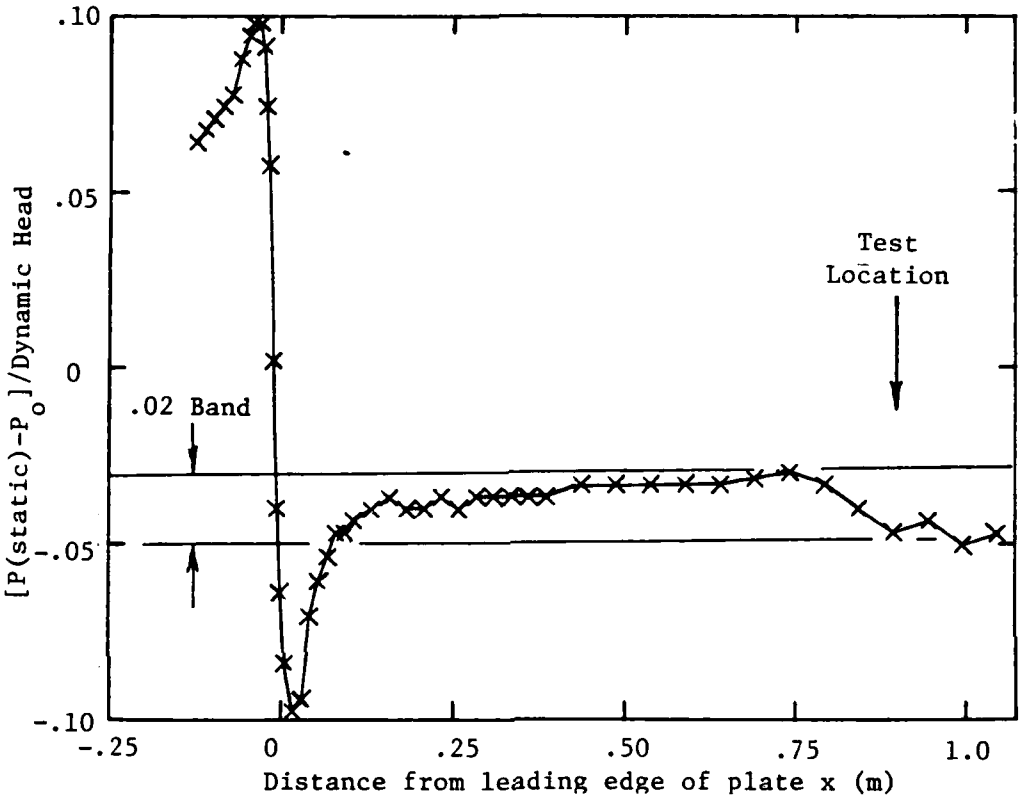

FIGURE 3.3 Longitudinal Pressure Variation

A flow visualization to check the effect of transverse wall turbulence was performed using Shapiro's technique, also used by Gedney. The results were identical to Gedney's as shown in Figure 3.4. The shear stress transducer was tested in the 7.6 cm (3 inch) hole at the location indicated.

The boundary layer was tripped to initiate turbulence by two thicknesses of duct tape 1 cm in width and 0.5 mm in total height. The tape was placed on the upper surface of the plate 2 cm from and parallel to the leading edge. According to the criterion developed by Gibbings [White (1976)], fully effective tripping to turbulent flow is assured if

$$\frac{U_\infty k}{\nu} \simeq 826 \qquad (3.1)$$

where k is the height of the surface roughness. In the present work, $k \simeq 0.5$ mm ensures immediate transition for free stream velocity greater than 25 m/s.

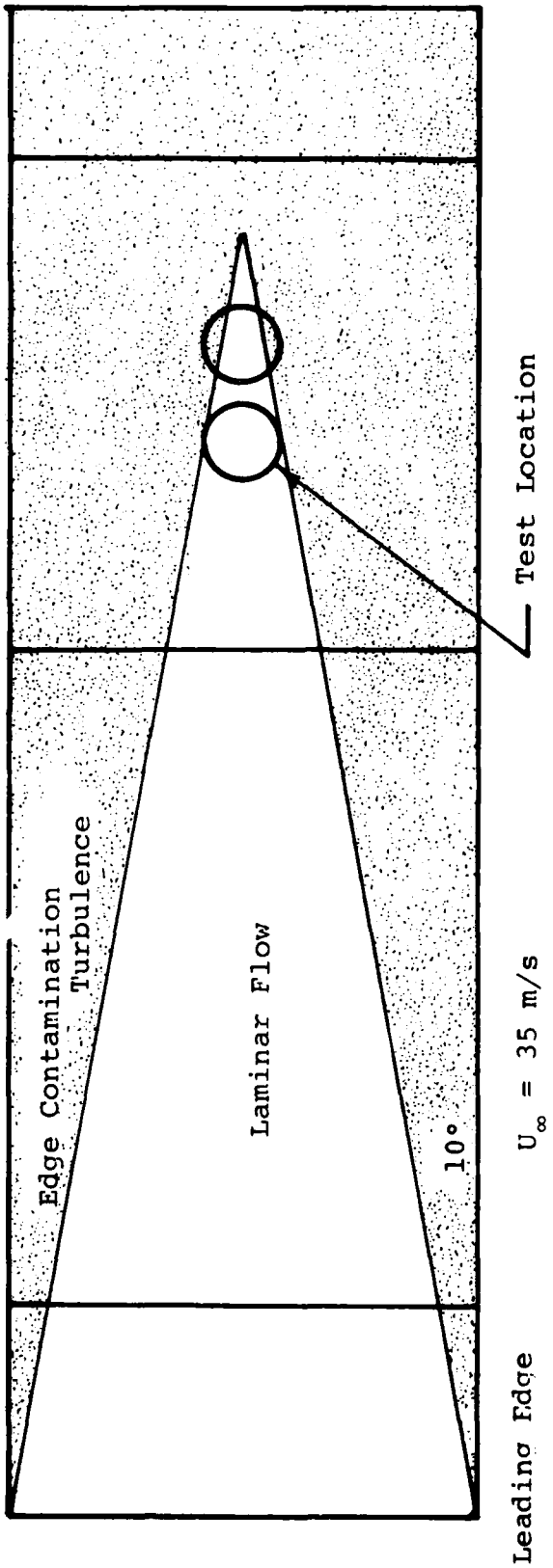

FIGURE 3.4 Flow Visualization - Extent of Edge Contamination [from Gedney (1979)]

3.3 FLOATING ELEMENT MISALIGNMENT

Allen (1977) has indicated that the major sources of error in floating element shear stress measuring devices are lip forces and normal forces which contaminate the friction force that the device is being used to measure. Lip forces are developed by a nonuniform pressure distribution around the periphery of the floating element caused by either flow through the gap around the element or misalignment of the floating element with respect to the wall. Normal forces introduce error when a nonuniform pressure distribution over the surface of the floating element shifts the normal force's center of effort, generating a moment which deflects the floating element.

Allen found that errors in the measured wall shear stress due to lip and normal forces can be larger than the actual wall shear stress by as much as a factor of 4. His results indicate that proper alignment of the floating element in the wall is the key factor in minimizing error, a finding corroborated by Burke (1984) who used a floating element to measure skin friction in the MIT water tunnel.

Proper alignment of the floating element in the wall is therefore critical in the current design, and was assured by measurement with a KD-45 Fotonic Sensor made by Mechanical Tech-

nology Incorporated. The Fotonic Sensor is a non-contact measuring device that projects several beams of light through fiberoptic strands and then measures the quantity of light reflected from an object to determine the distance to the object. The Fotonic Sensor was used in its less sensitive range (±2 μm) to determine that the floating element protruded 9 μm from the wall (y^+ = 0.69), which was judged to be satisfactory.

3.4 INCLINATION RESPONSE

Experimental verification of the transducer's response to inclinations from the vertical were made, as shown in Figure 2.6. The transducer was attached to the mid-span of a sturdy 1.83 m long aluminum I-beam which was raised or lowered at one end a known distance to generate inclination angles smaller than one degree. An inclination angle of one degree is obtained when one end of the I-beam is 32 mm higher than the other end, so it is possible to maintain accuracy to about 0.01 degree. The effect of I-beam flexure on inclination angle is small to begin with and further reduced by placing the transducer at the I-beam's mid-span, so that I-beam flexural effects have been neglected.

3.5 INSTRUMENTATION

3.5.1 Dynamic Characteristics

Transducer dynamic characteristics were investigated using the instrumentation shown in Figure 3.5. The transducer was mounted in a phenolic bracket and secured to the vibration exciter so that the transducer could be shaken either in the plane of the wall or normal to the wall. As shown in Appendix A.2, the transducer's response to acceleration of its base and its response to a shear force acting on the floating element are dynamically equivalent, although caution must be exercised in interpreting results since the acceleration of the transducer's base also introduces an effective force along the length of the cantilever plate which is absent during normal operation of the transducer. An accelerometer, calibrated using a General Radio model 1557-A vibration calibrator, was attached to either the phenolic bracket or to the transducer body to measure the vibration of the transducer body. A Hewlett-Packard 5423A structural dynamics analyzer was used to generate the random noise excitation of the vibration exciter and also to calculate the transfer function between the transducer output and transducer body acceleration. The spectrum of the random noise excitation was shaped using an MXR 31-band equalizer so that the spectrum of the transducer body acceleration was approximately uniform over the frequency band of

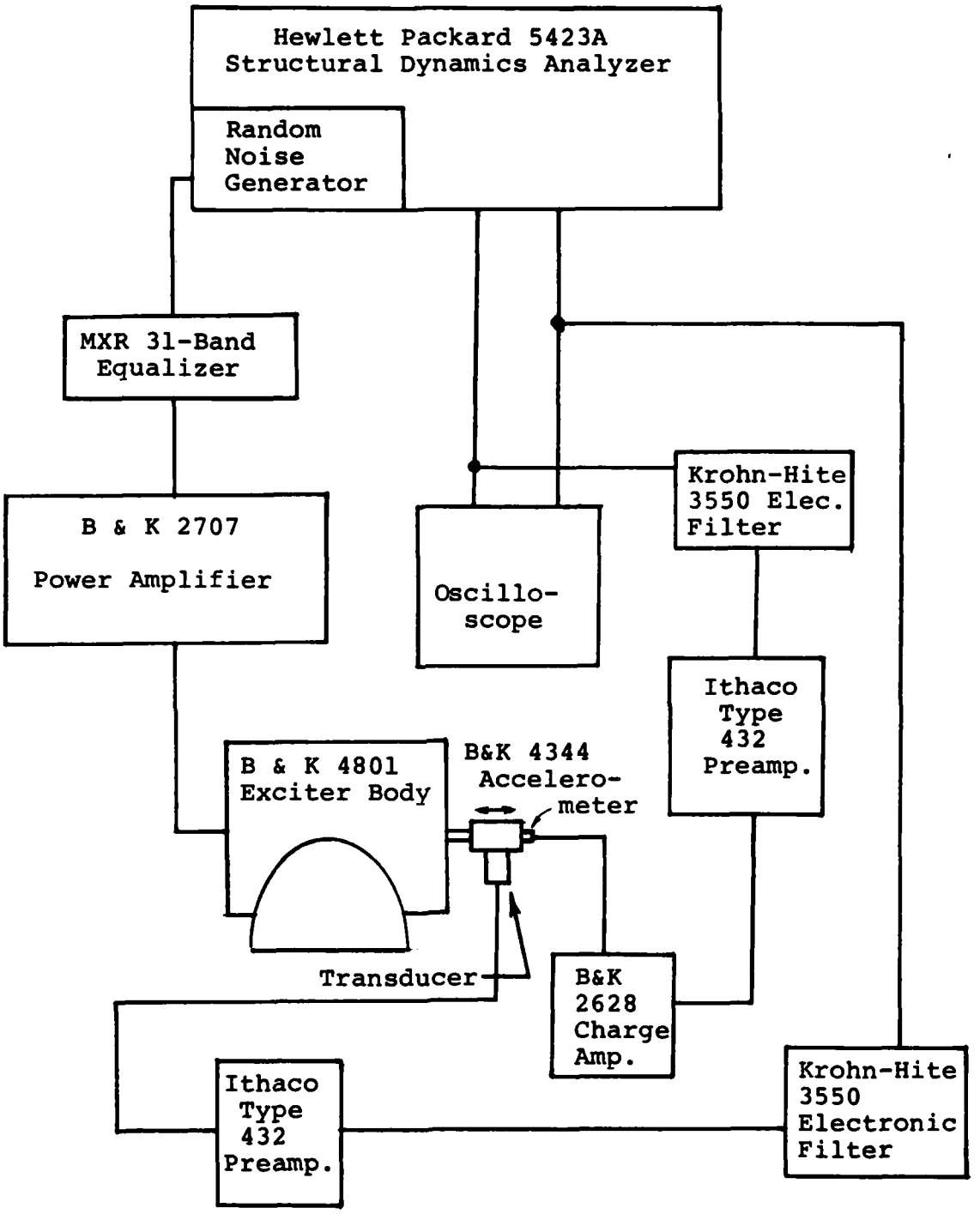

FIGURE 3.5 Instrumentation - Dynamic Characteristics

interest.

3.5.2 Test Conditions

The free stream velocity into the test section was monitored by measuring the pressure drop across the wind tunnel contraction section with a Betz micromanometer. A calibration was performed by Shapiro (1977) to ensure an accuracy of 0.1 m/s.

The longitudinal pressure variation along the test plate was measured using a small static pressure tube (United Sensor and Control Corp. PSA-16) and a Validyne DP15-24 differential pressure transducer. A Validyne model CD23-1071 electronic manometer powered the pressure transducer and provided a digital readout of the differential pressure in millimetres of water.

Mean velocity profile measurements were performed using a hot wire anemometer probe (Thermo-Systems Inc. probe model 1261-T1.5) with a Disa model 55005 battery-powered constant temperature anemometer and a linearizer built by Moeller using an Analog Devices 433B programmable function generator. The hot wire probe was calibrated against a pitot tube used with the Validyne DP15-24 differential pressure cell. Mean velocity was measured on a digital voltmeter after being filtered by a 0.1 Hz active low pass filter built by Lueptow (1984).

3.5.3 Transducer Calibration

Wall shear stress transducer electronics were calibrated using a General Radio model 1210-C function generator in conjunction with a Hewlett-Packard model 5532A electronic counter and a digital voltmeter. With gain of the AD524 instrumentation amplifier set at 10, the gain of the frequency to voltage converter was adjusted so that a change in input frequency of 500 Hz (from 55.6 kHz to either 55.1 kHz or 56.1 kHz) produced a change in output voltage of approximately 5.0 V. The exceptional sensitivity of the transducer made workbench calibration of the entire transducer unfeasible, so the transducer was calibrated against the law of the wall in situ.

3.5.4 Wall Shear Stress

The wall shear stress was measured using the instrumentation of Figure 3.6. Coherence between the acceleration of the transducer and transducer output was monitored using the structural dynamics analyzer to ensure that transducer acceleration did not significantly affect transducer output. The structural dynamics analyzer was also used in its time record mode to make long-period zero drift measurements.

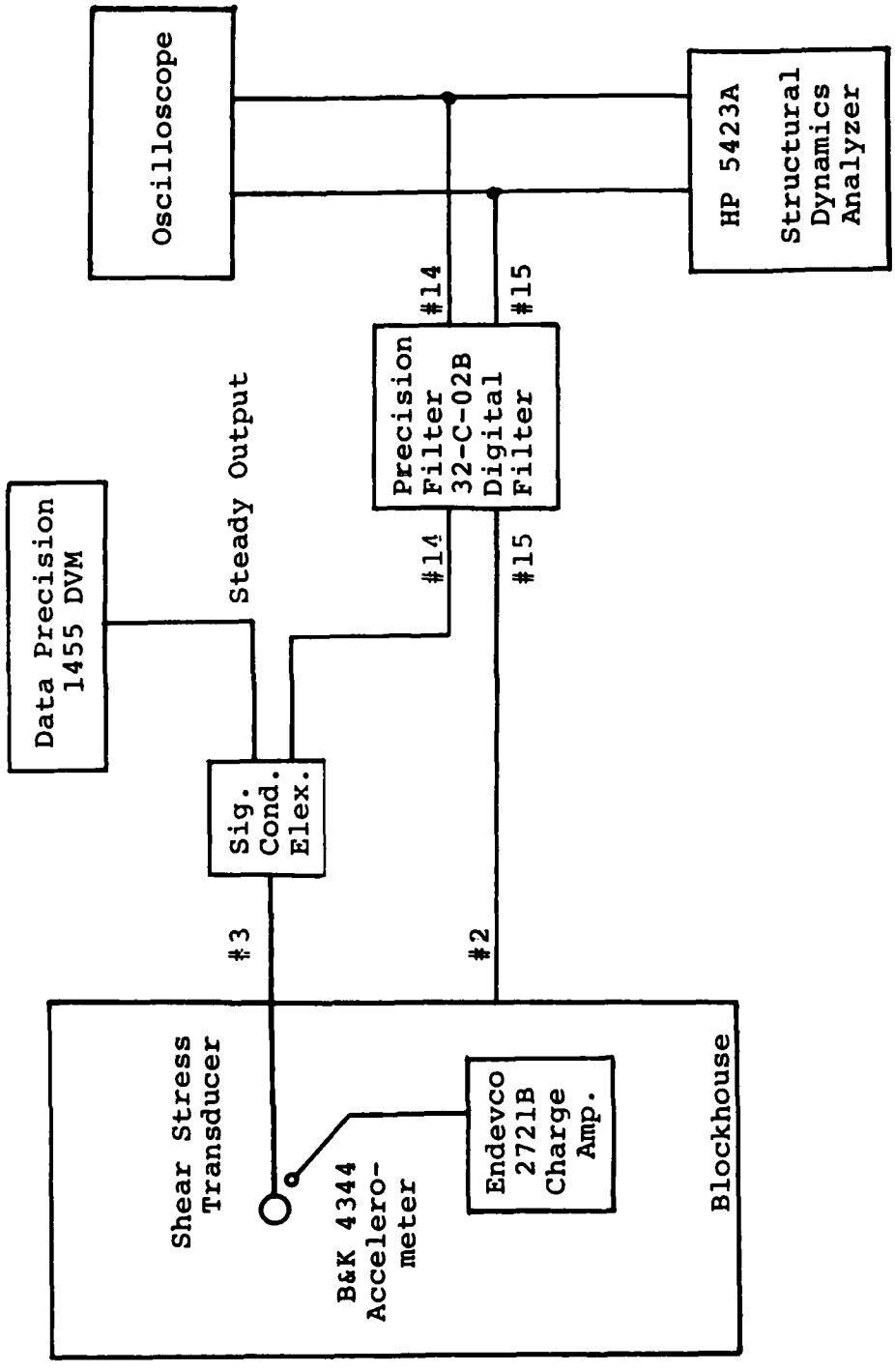

FIGURE 3.6 Instrumentation - Wall Shear Stress

4. EXPERIMENTAL RESULTS AND DISCUSSION

4.1 DYNAMIC CHARACTERISTICS

Transducer dynamic characteristics were evaluated for two different transducer configurations: one with a seal in the gap surrounding the floating element and another with the gap unsealed. For brevity, these two configurations will be referred to as the "sealed" and "unsealed" configurations, respectively. Investigation of the dynamic characteristics of the two gap configurations was conducted in two phases. In the first phase, the accelerometer used to measure transducer body acceleration was attached to the phenolic bracket mounting the transducer to the vibration exciter. This test configuration permitted the rotation of the transducer in the bracket and was used to verify that the transducer can discriminate against signals orthogonal to its sensitive axis in the plane of the wall, but introduced errors in that the accelerometer was not mounted directly on the transducer body. The second phase utilized an accelerometer attached directly to the transducer body in the location indicated on Figure 2.2. In this later phase, attention was devoted exclusively to improving understanding of the dynamics of the transducer in its sensitive direction, the orthogonality of the device having already been demonstrated.

Phase 1. The sealed configuration in the initial phase used as the gap sealing material an epoxy, ECCOGEL 1365-15, made by Emerson and Cuming. Measuring only 15 on the Shore hardness scale commonly used in the polymer industry, the epoxy is very soft but is nearly incompressible. Owing to the manner of the transducer's construction, it was not possible to determine the geometry of the gap seal beneath the surfaces of the adapter and floating element after the epoxy cured.

The transfer function between the transducer output and the transverse acceleration of the transducer body is shown in Figure 4.1 (unsealed configuration) and Figure 4.2 (sealed configuration). The magnitude plots are normalized on the peak magnitude of the unsealed transducer's transfer function in order to highlight the order of magnitude loss in response caused by the epoxy seal in the gap. The fundamental resonant frequency of the unsealed transducer (Figure 4.1) is approximately 63 Hz, very close to the 61.7 Hz predicted during design. Figure 4.2 indicates that the addition of the epoxy seal leads to an increase in the fundamental resonant frequency to about 360 Hz as well as an apparent reduction in sensitivity.

The apparent loss of sensitivity is misleading. Table V (Appendix B) lists the resonant frequencies for the first three vibration modes of the beam element subjected to clamped-free, clamped-pinned, and clamped-clamped boundary conditions. The ob-

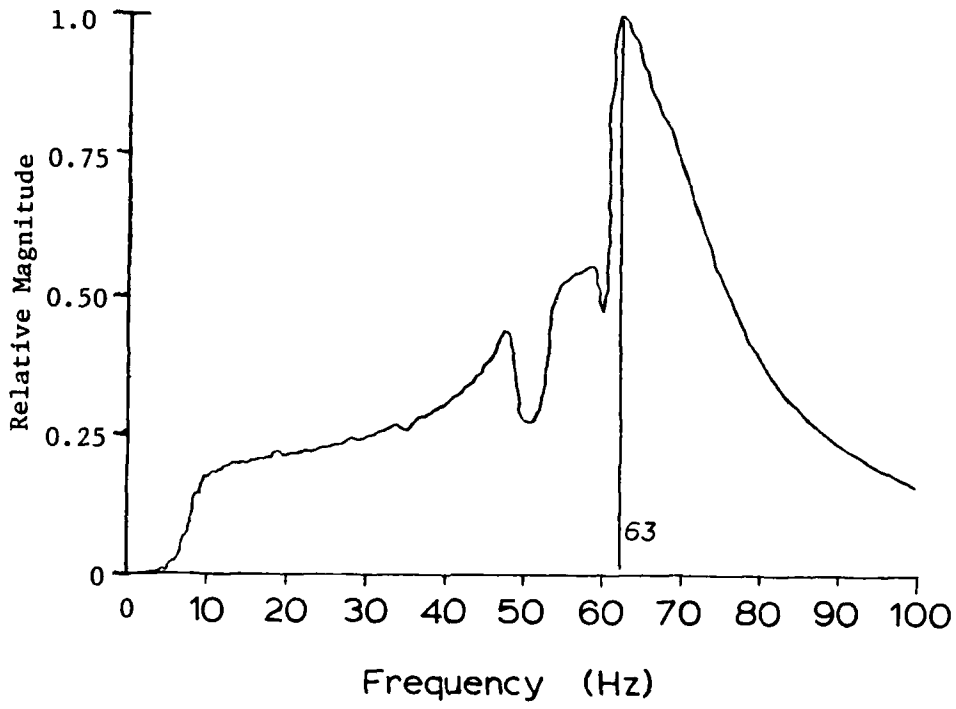

a. Magnitude relative to unsealed maximum

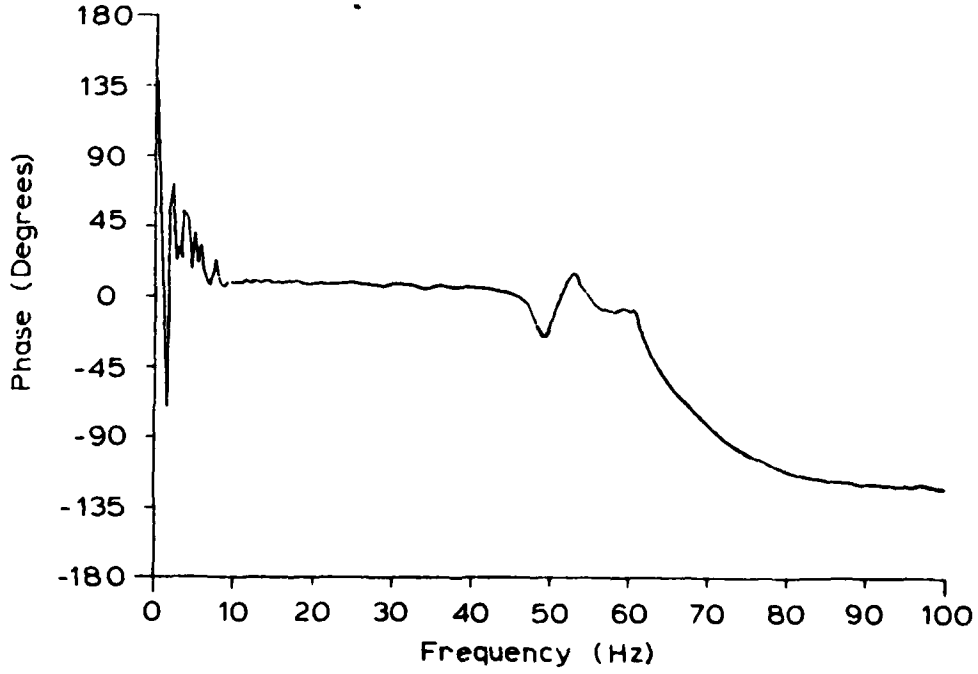

b. Phase Angle

FIGURE 4.1 Initial Transfer Function - Gap Unsealed

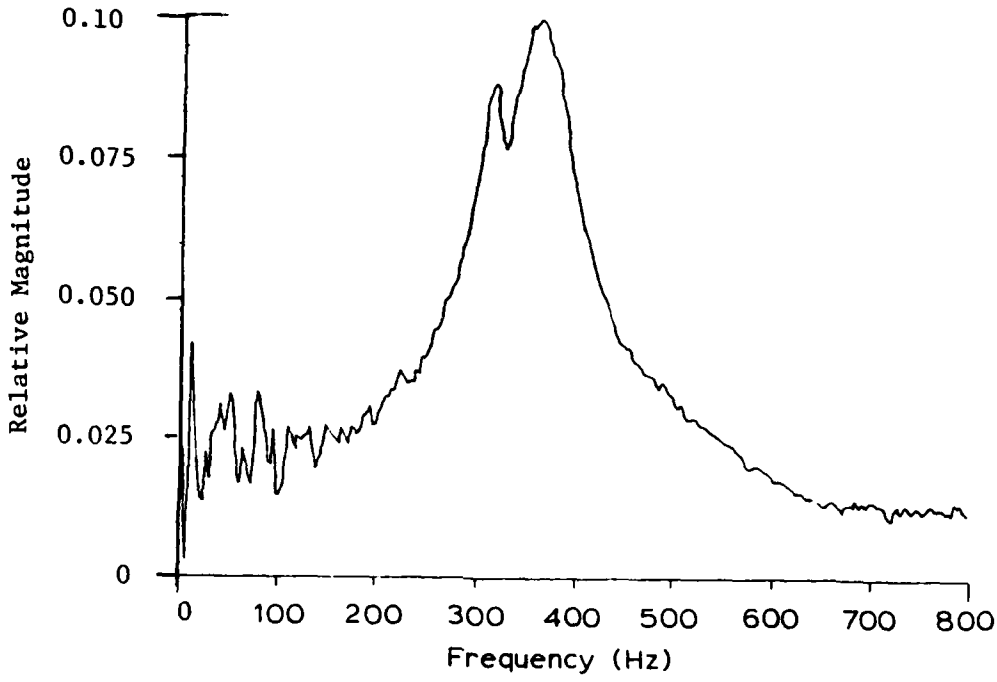

a. Magnitude relative to unsealed maximum

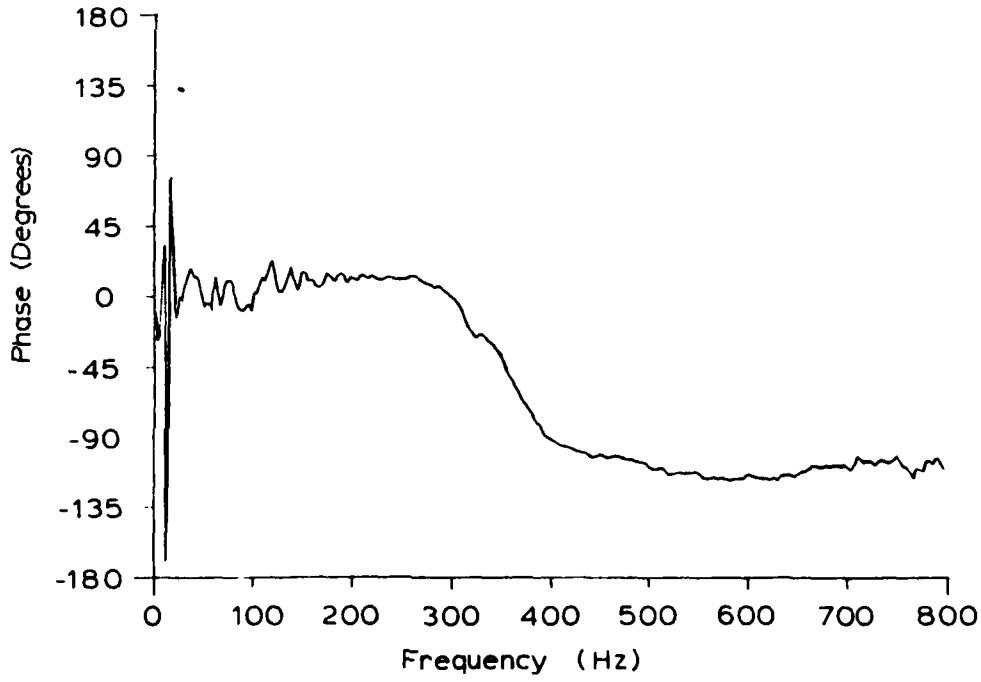

b. Phase Angle

FIGURE 4.2 Initial Transfer Function - Gap Sealed

served fundamental resonant frequency of the sealed transducer (360 Hz) is bracketed by that of a clamped-pinned beam element (341 Hz) and a clamped-clamped beam element (494 Hz), neglecting the rotational inertia of the floating element which was found to be insignificant. This suggests that the beam element in the sealed configuration exhibits a pinned condition at the floating element or, more correctly, a mixed condition that is a hybrid of pinned and clamped conditions but closer to pinned. If such is the case, then the sealed transducer does not respond to wall shear stress, since the floating element is located at a node of the beam element's response and therefore never translates. The sealed transducer is thus incapable of responding to forces applied to the floating element, but rather responds only to forces applied to the cantilever plate. This is shown in Figure 4.2, where the transducer is responding to the D'Alembert or inertia force $- \mu \frac{d^2 z_o}{dt^2}$ (using the notation of Appendix A.2) produced on the cantilever plate by the transverse acceleration of the transducer base. The use of a seal in the gap around the floating element is self-defeating in this instance, eliminating transducer response to the wall shear stress.

The resonances of both the sealed and unsealed configurations exhibit considerable damping, approximately 14 percent of critical damping in each case. The unsealed configuration's response in Figure 4.1a shows an irregularity at 60 Hz caused by noise from the field windings of the vibration exciter, while the

poor response below 10 Hz is due to a low frequency limitation of the vibration exciter. The phase angle of both configurations' transfer function is anomalous, since it does not change by 180 degrees as it should when passing through an isolated resonance. The irregularity in Figure 4.1a near 50 Hz and the similar irregularity in Figure 4.2a near 325 Hz are also strange, but may be due to the vibration of the bracket securing the transducer to the exciter.

Phase 2. The second phase of the investigation of transducer dynamics was undertaken to resolve some of the issues raised concerning the phase of the transfer function and the role of the mounting bracket in introducing the anomalies encountered in the earlier phase. Also of interest was confirmation of the hypothesis that the floating element in the sealed configuration was effectively held motionless by the seal. In this phase, the accelerometer used to measure transducer transverse acceleration was mounted directly on the phenolic transducer assembly rather than on the bracket mounting the transducer to the vibration exciter. For the "sealed" configuration, a single piece of standard vinyl electrical tape was securely attached to the surfaces of the floating element and adapter to approximate a pinned boundary condition at the floating element.

Figures 4.3 and 4.4 illustrate the transfer function

obtained between the transducer output and the transverse acceleration of the transducer body. The units of the ordinate in the magnitude plot are volts per g, where 1 g = 9.8 m/s^2 is the acceleration due to gravity.

The unsealed configuration's transfer function (Figure 4.3) is virtually identical to Figure 4.1, with the following important exceptions:

- the phase is well-behaved and very properly shifts through 180 degrees when passing through the resonance;
- the anomaly in the magnitude near 50 Hz has vanished, as expected; and
- the irregularity in magnitude at 60 Hz is sharper than that encountered earlier, and gives rise to slight irregularities at 120 Hz and 180 Hz.

As discussed earlier, the noise at 60 Hz (and multiples thereof) is due to the field windings in the vibration exciter. The slight irregularity in magnitude at 100 Hz is due to noise from the vibration exciter's blower motor.

The "sealed" configuration's transfer function is remarkably similar to that of Figure 4.2, despite the difference between the two seals (electrical tape as opposed to epoxy). In Figure 4.4:

- the fundamental resonant frequency has increased to 375 Hz (from 360 Hz in Figure 4.2);
- the damping has decreased to 7 percent of critical (in

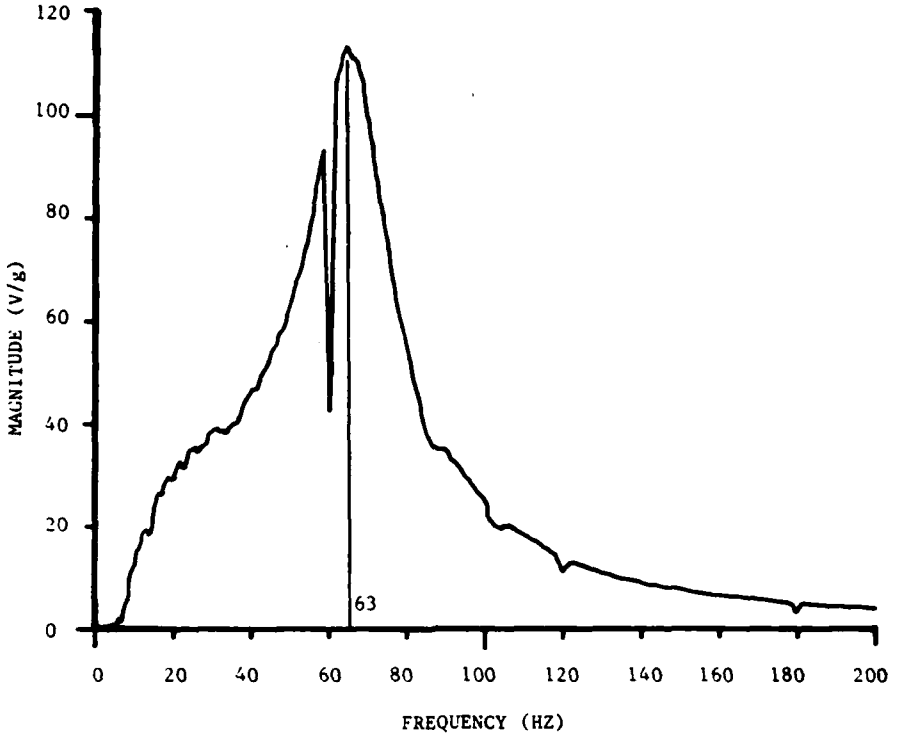

a. Magnitude

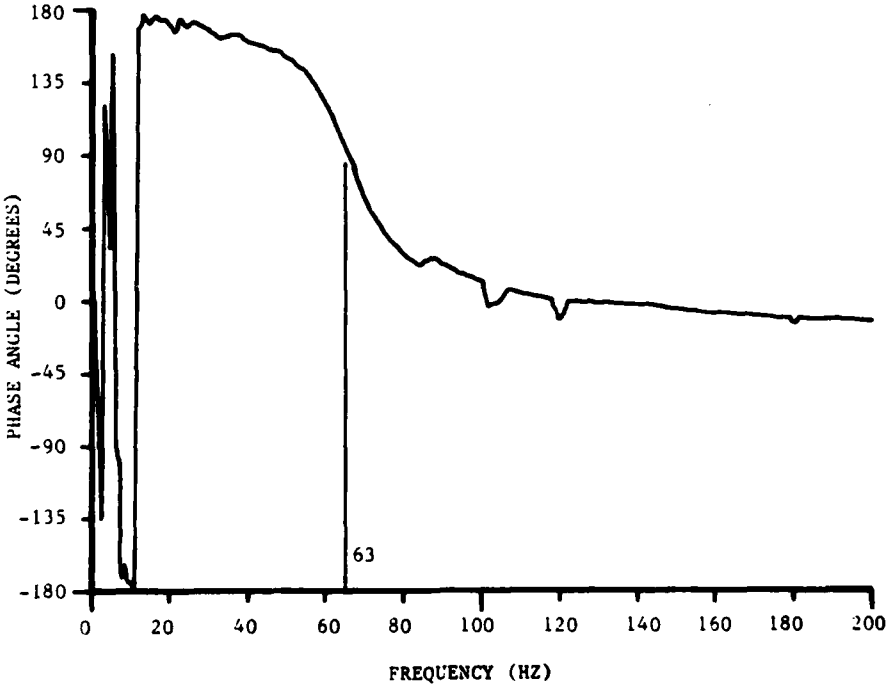

b. Phase Angle

FIGURE 4.3 Final Transfer Function - Gap Unsealed

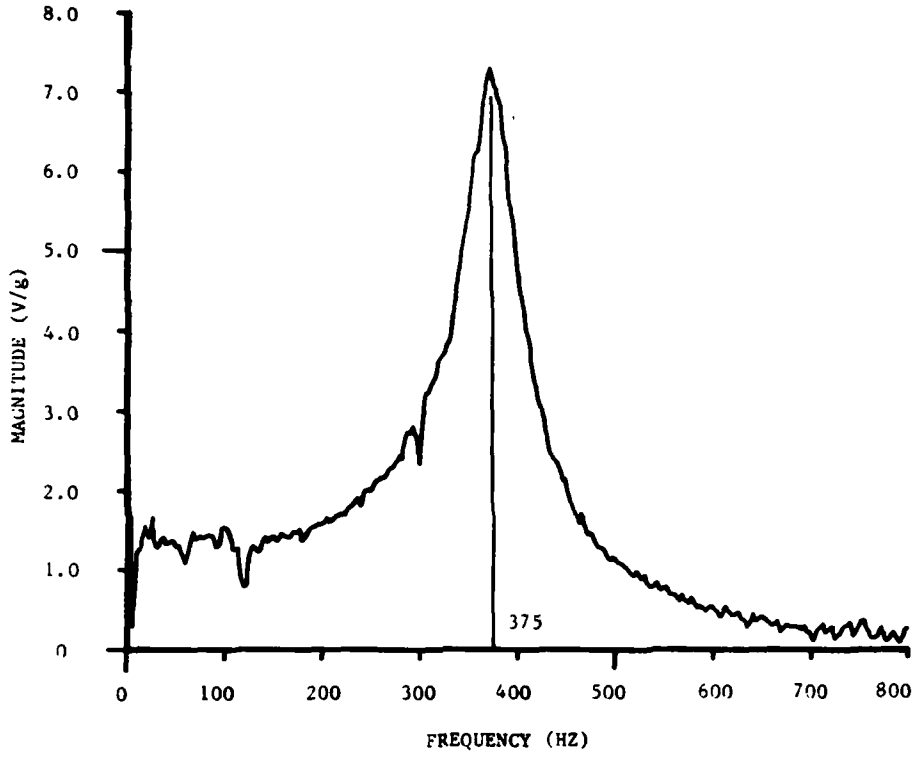

a. Magnitude

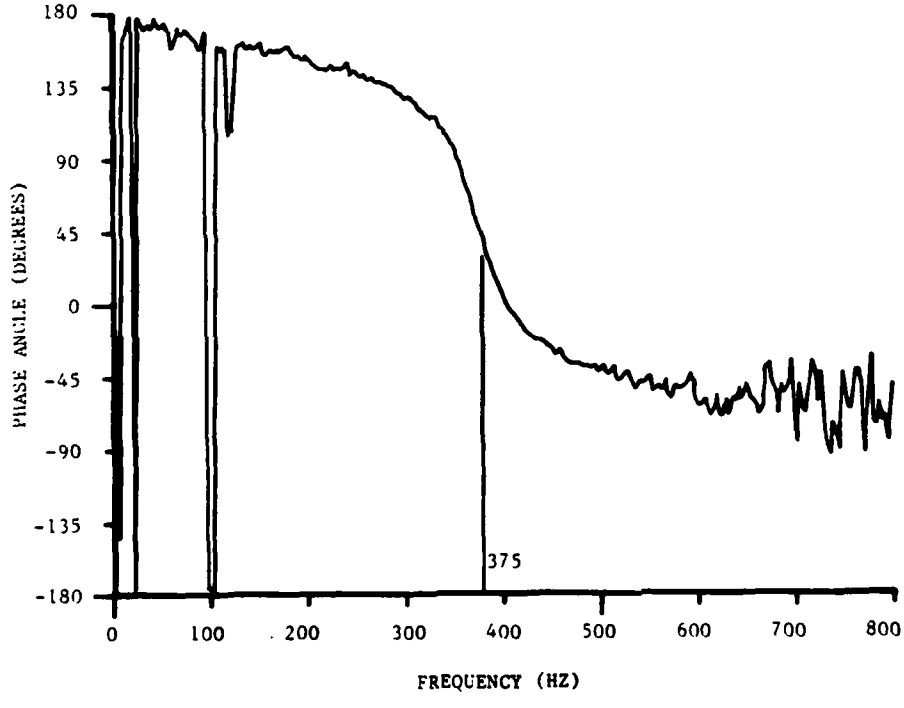

b. Phase Angle

FIGURE 4.4 Final Transfer Function - Gap Sealed

contrast to 14 percent in Figure 4.2);

- the large irregularity in magnitude just below resonance has vanished; and
- the phase is well-behaved and shifts through 180 degrees through the resonance.

The results of this phase of the investigation indicate that the anomalies encountered were indeed experimental and confirm the hypothesis that the gap seal immobilizes the floating element in translation.

4.2 WALL SHEAR STRESS

4.2.1 Law of the Wall

The law of the wall was used to obtain estimates of the mean wall shear stress for comparison with the steady mean wall shear stress measured by the transducer. Mean velocity profiles were measured above the floating element with a hot wire probe at free stream velocities of 26.0 m/s, 30.5 m/s, and 34.5 m/s corresponding to momentum thickness Reynolds numbers of 3140, 3500, and 3760. The velocity profiles were analyzed using the FORTRAN program BLPROF2 in which the user iteratively guesses the friction velocity U_τ and the location of the wall (in the measured coordinates) until the measured data coincides in the inner region of the profile with Musker's explicit formula for the turbulent mean velocity profile [see Musker (1979)]. BLPROF2 permits the user to fair the measured data into the wall using Musker's formula and then integrates the resulting faired profile using trapezoidal rule to obtain displacement thickness δ^* and momentum thickness θ .

The three mean velocity profiles are plotted in Figure 4.5 nondimensionalized on inner parameters of the boundary layer. It can be seen that the velocity profile for $Re_\theta = 3500$ contains little or no wake, whereas the other two profiles exhibit a noticeable wake. The velocity profile at $Re_\theta = 3500$ was measured

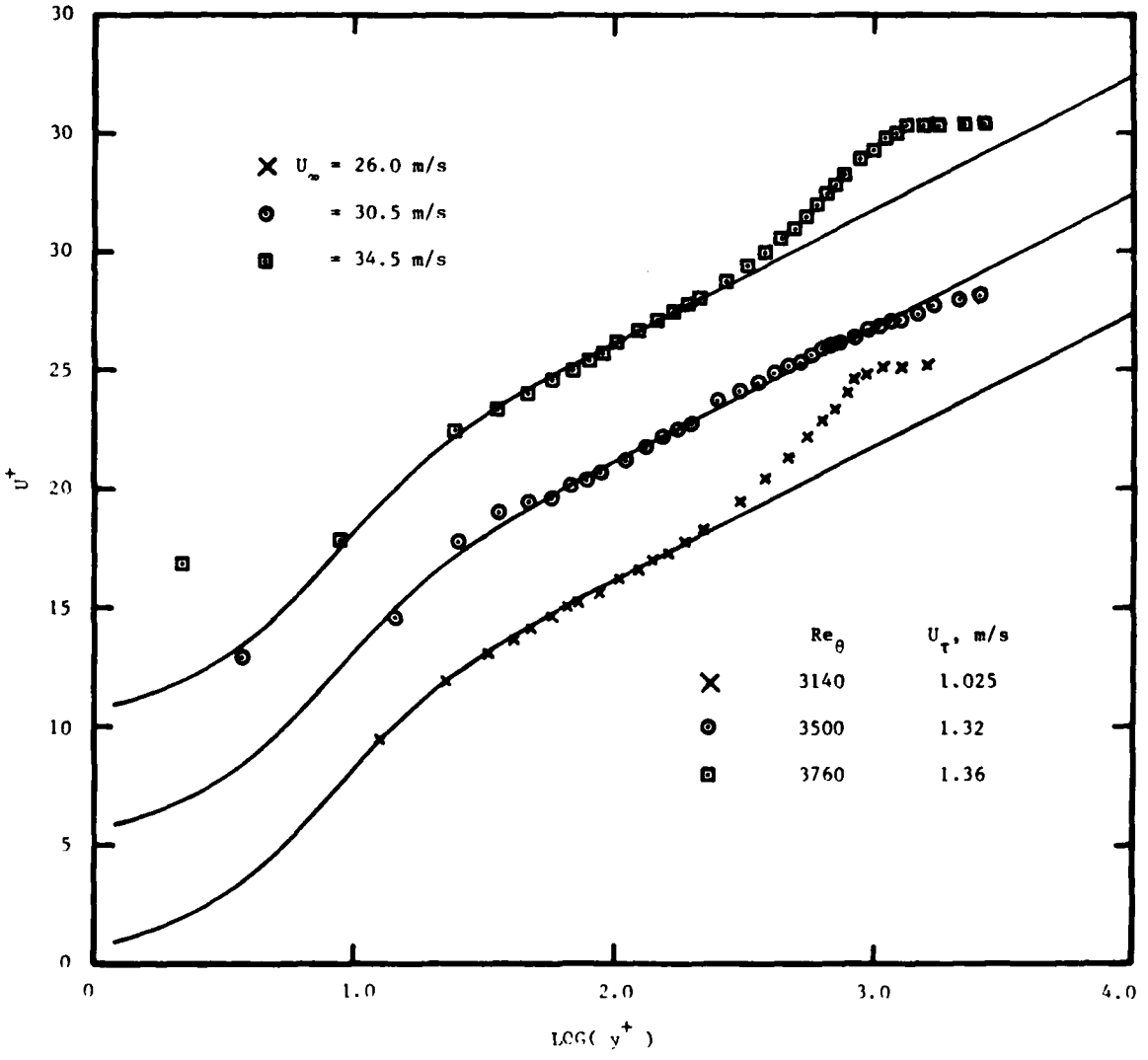

FIGURE 4.5 Mean velocity profiles in semilogarithmic coordinates. Ordinate scale refers to lowest curve; other curves successively displaced upward by 5.0 units.

during a different test period than the velocity profiles at Re_θ = 3140 and 3760, highlighting the difficulty of reproducing test conditions exactly. Since the anomaly in the wake at Re_θ = 3500 does not affect the logarithmic overlap region, the change in the outer flow causing the different wake is expected to have little effect on the wall shear stress. Because all three mean velocity profiles collapse to the classical turbulent mean velocity profile, it is assumed that each boundary layer exhibits fully developed turbulence despite being tripped into turbulence so that the application of the law of the wall is valid.

4.2.2 Transducer Measurement

Steady. Steady mean wall shear stress was measured by the transducer at the same Reynolds numbers as the velocity profiles; the results are listed in Table IV, where they are compared to the results obtained from the law of the wall. Both the law of the wall data and the transducer-measured data are plotted in Figure 4.6, taken from skin friction data analyzed by Murlis, et. al., (1982). Transducer measurements at Re_θ = 3140 and 3500 are excellent, while that for Re_θ = 3760 is a bit high but still within experimental uncertainty, estimated in Appendix C to be 66 percent. The acceleration of the transducer was neglected in analyzing transducer output, since low coherence between the two (at most 10% to 20%) indicated that there was little systematic

relationship between the transducer output and acceleration of the transducer body.

TABLE IV
Results

Re_θ	3140	3500	3760
$\bar{\tau}_{law\ of\ the\ wall}$	1.25 Pa	2.05 Pa	2.20 Pa
$\bar{\tau}_{measured}$	1.3 Pa	1.7 Pa	3.1 Pa

Transducer zero drift was surprisingly low despite the transducer's extreme sensitivity, averaging 20% of the mean signal over the period of the measurement (1 to 1.5 minutes). Zero drift was measured by covering the floating element with an index card while the wind tunnel was running at the proper speed. A short length of wire 0.5 mm in diameter was taped beneath the card as a spacer to keep the card from contacting the floating element. Sample plots of the zero drift measured by the structural dynamics analyzer over a period of 1 minute are shown in Figure 4.7 where they are compared to the mean output voltage determined by subtracting the average reference voltage from the ansducer total output voltage. Each data run took 3 to 4 minutes from the start of the initial zero measurement to the measurement of the wall shear stress and the concluding zero measurement.

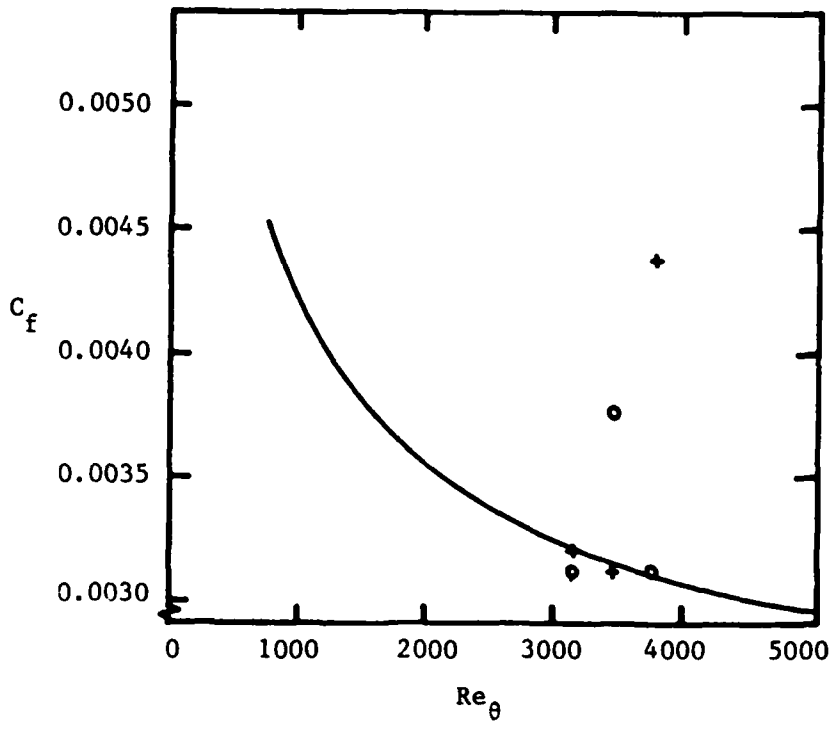

FIGURE 4.6. Skin friction coefficient variation with momentum thickness Reynolds number [from Murlis, et. al., (1982)] : +, measured data using wall shear transducer; o, data from law of the wall.

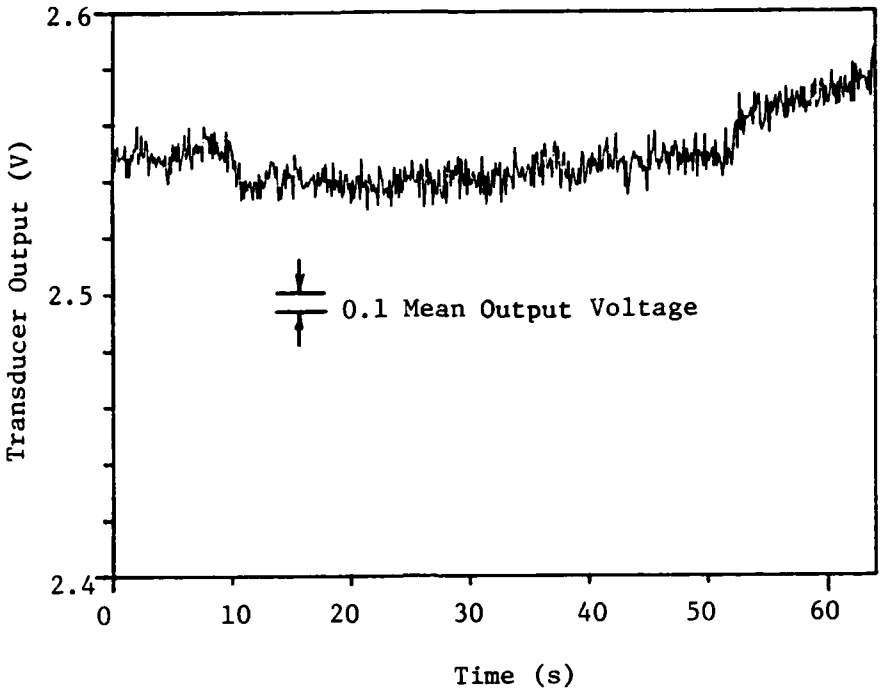

a. Re_θ = 3140

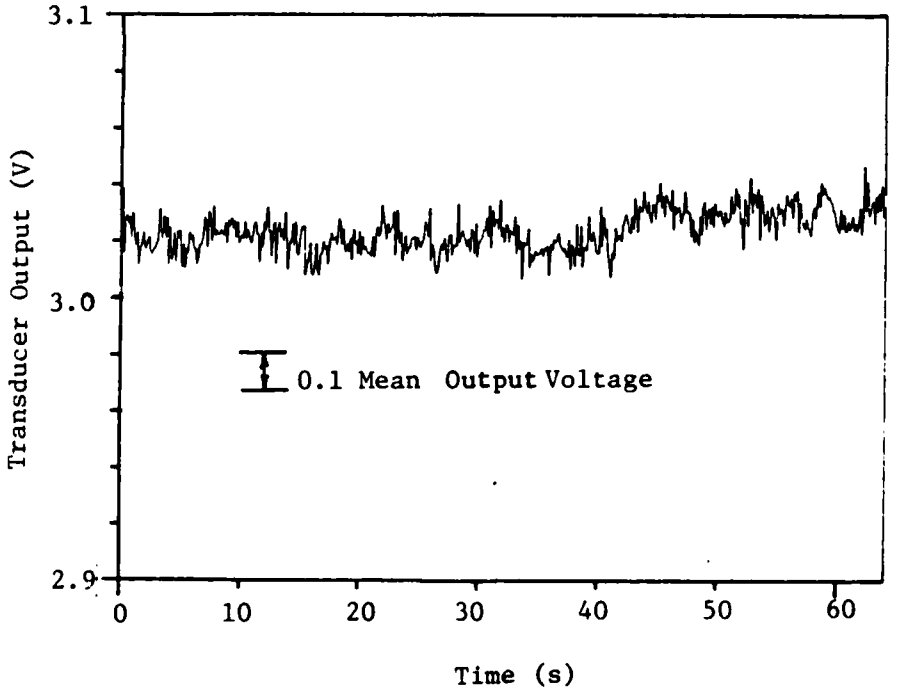

b. Re_θ = 3760

FIGURE 4.7 Zero Drift

Unsteady. The unsteady mean wall shear stress spectrum for Re_θ = 3140 and 3760 is shown with the background spectrum in Figure 4.8. Although the plots show some dynamic character of the unsteady wall shear stress, they show little of its structure owing to the low resonant frequency of the transducer. If it is assumed that an instrument is usable up to a frequency one order of magnitude less than its first natural frequency, then the transducer can only be used up to 6.3 Hz. Burton (1974) indicates that the frequency related to sublayer bursting in a turbulent boundary layer is given approximately by

$$\frac{f\ \delta^*}{U_\infty} \simeq 0.03 \qquad (4.1)$$

where δ^* is the displacement thickness. For the conditions under which the transducer was tested, equation 4.1 predicts the burst frequency to be about 300 to 500 Hz, well above the nominal bandwidth of the transducer and thus unmeasurable.

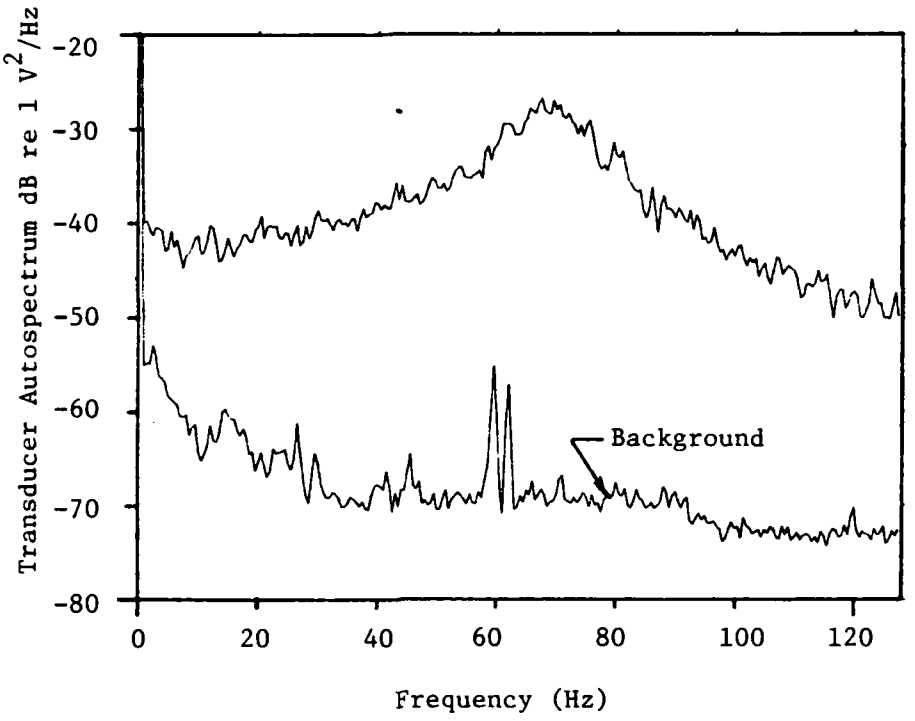

a. Re_θ = 3140

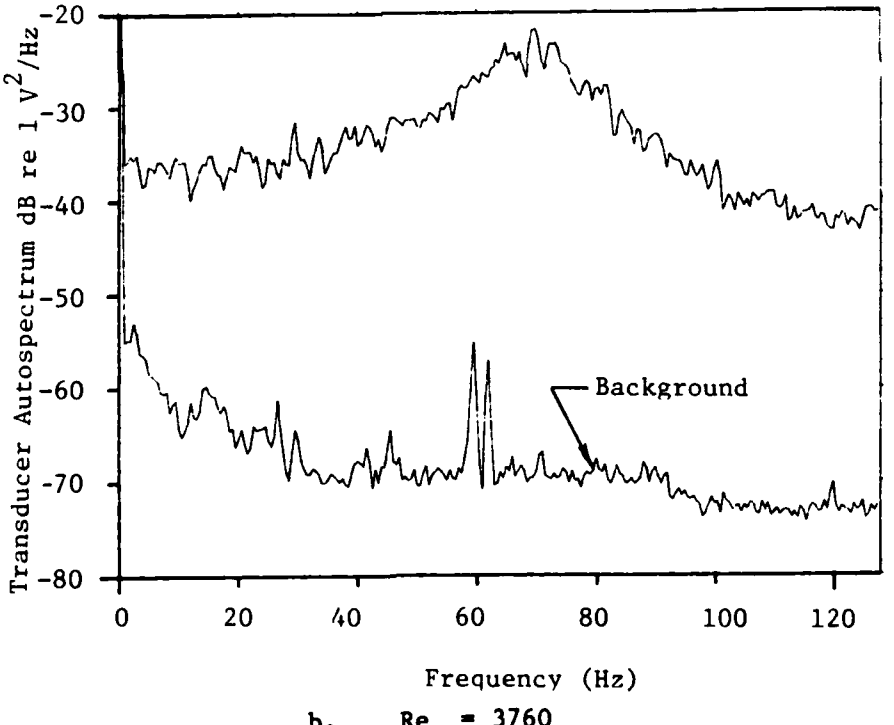

b. Re_θ = 3760

FIGURE 4.8 Wall Shear Stress Spectral Density

5. RECOMMENDATIONS

In the short term, the wall shear transducer is usable for measuring the steady mean wall shear stress. The sensitivity of the device is so great, however, that calibration must be performed in situ, preferably in a laminar boundary layer where the wall shear stress is well known. The electronics should be upgraded by the installation of precision instrumentation amplifiers to replace the commercial-grade amplifiers currently in use. This should reduce the high frequency noise observed at the transducer output and improve the stability of the astable multivibrator, whose center frequency was observed to drift from 55.6 kHz to 46.5 kHz over seven days of continuous operation.

Long range plans for the transducer should include increasing its bandwidth, decreasing its sensitivity to inclination, and gaining an understanding of how the gap around the floating element affects the shear stress measurement (given that the gap cannot be sealed, as the current research suggests).

As regards the bandwidth, the first resonant frequency of the beam element needs to be increased at least two orders of magnitude so that the transducer can measure frequencies near the burst rate. A larger bandwidth is desirable so that the device

can always be used more than an order of magnitude below its fundamental resonance, which is far less complicated than attempting to use an instrument through its first resonance. The transducer should be as simple to use as possible. The linearity of the transducer, coupled with sufficient bandwidth, will make it a powerful instrument for measuring the dynamics of the wall shear stress. As linear system theory demonstrates, only in a linear system can the statistics of an output (such as transducer output voltage) be related definitively and unambiguously with statistics of the input (such as wall shear stress).

Next, the sensitivity of the transducer to inclinations from the vertical should be reduced by at least two orders of magnitude so that inclination has a second-order effect on transducer output (it is assumed that the steady transducer signal is zeroth-order while the unsteady signal is first-order). Coupled with the need to maintain roughly the same sensitivity to wall shear stress s_τ, the requirements for an improved physical design imply that the mass of the floating element and capacitor plate must be reduced several orders of magnitude. If the size of the floating element is reduced, then equation 2.3 indicates that $\frac{f_o\ G}{k_s\ d_o}$ must be increased a compensating amount to maintain the desired s_τ. Decreases in k_s require further decreases in mass in order to maintain the required bandwidth. Increases in G lead to only marginal improvements in transducer performance since noise is generally amplified along with the signal.

Finally, and most important, a better understanding of the role of the floating element gap in affecting the boundary layer must be reached. There is little in the literature that sheds any light on this issue. Allen (1977) identified that small gaps increase the sensitivity of the floating element transducer to errors introduced by misalignment of the floating element with the wall. Winter (1977) mentions that the effect of gaps perpendicular to the flow is poorly understood, but that the effect of the gap should be negligible if the gap width is smaller than 100 in wall coordinates. McMichael, et. al., (1979) found that a transverse slot in the wall of a turbulent flow affects the boundary layer downstream of the slot. In the authors' words, "Evidently, temporary release of the no slip condition as the boundary layer passes over the slot results in a local decrease in turbulence production as indicated by the weakened intensity near the wall just downstream of the slot." (p. 417). Since the gap is adjacent to the wall area where the shear stress will be measured, it is unclear whether or not the boundary layer will "heal" itself sufficiently to permit an unbiased measure of the wall shear stress, particularly if the measurement area is small. The effect of the gap is a fundamental issue which has not yet been adequately addressed.

The most fruitful course of action appears to be the microminiaturization of the transducer to a scale where a very small

gap and precise alignment of the floating element can be maintained. Peterson (1982) discusses the merits of unicrystalline silicon dioxide at great length; small cantilever beams 8 μm long, 2 μm wide, and 0.1 μm thick with a fundamental resonant frequency of 1.2 MHz have already been made from the material. A microminiaturized wall shear stress transducer with such a small cantilever, using the capcitance-measuring technique outlined in the current research, has a number of distinct advantages. A floating element with sensing area 2 μm by 0.1 μm would have superb spatial resolution, excellent sensitivity, and a large bandwidth. The considerable reduction in mass would greatly reduce the sensitivity of the device to inclination. Further, it should be possible to keep the gap around the floating element on the order of about 10 angstroms so that the gap has a negligible effect on the flow. Precise alignment of the floating element is possible on the microscopic scale, which may circumvent the extreme sensitivity of the floating element to misalignment-induced errors when the gap is small. Recent trends suggest that such a transducer could be mounted on a 20 μm chip with its own accelerometer and compensation network, permitting an array of such transducers to measure the spatial distribution of the shear stress over the surface of the wall.

6. CONCLUSIONS

The development of a passive floating element wall shear stress transducer using a sensitive capacitance-measuring technique has been presented. In particular, the viability of using a frequency modulation scheme to perform the capacitance measurement has been demonstrated. The electronic sensitivity is such that the transducer is able to measure a 0.1 μm displacement of the floating element. Expected motions of the floating element are less than 5 μm and should not adversely affect the character of the boundary layer in which the measurement is made. The device is highly linear, enhancing its attractiveness for dynamic wall shear stress measurements.

The transducer has been tested and found to predict the steady mean wall shear stress to within the limits of experimental uncertainty (66%); two of the three data points obtained were within 2 percent of the actual steady mean wall shear stress. The transducer must be calibrated *in situ* in order to reduce the experimental uncertainty; workbench calibration is not feasible because of the transducer's exceptional sensitivity. The current transducer is not practical for dynamic measurements of the mean wall shear stress since it does not possess adequate bandwidth.

The gap around the floating element has been verified as being the greatest single vulnerability of the floating element transducer. It is not possible to seal the gap, since a gap seal in the current design immobilizes the floating element and prevents transducer response to wall shear stress. On the other hand, an open gap affects the boundary layer and introduces errors of its own to the wall shear stress measurement. Fundamental research is needed in this area in order to fully understand the gap effect.

Finally, a course of action has been recommended to improve the capabilities of the wall shear transducer so that it is practical for dynamic measures of the shear stress. In order to increase bandwidth, reduce transducer sensitivity to inclination, and minimize the adverse effects of the gap, the transducer should be microminiaturized. Microelectronics technology is becoming increasingly capable, and can already maintain the necessary sub-micron tolerances.

REFERENCES

Allen, J.M. 1977 "Experimental Study of Error Sources in Skin-friction Balance Measurements," ASME Journal of Fluids Engineering, March 1977, pp. 197-204.

Allen, J.M. 1980 "Improved Sensing Element for Skin-Friction Balance Measurements," AIAA Journal, vol. 18, no. 11, November, 1980, pp. 1342-1345.

Blevins, R.D. 1979 Formulas for Natural Frequency and Mode Shape, Van Nostrand Reinhold, New York.

Burton, T.E. 1974 "The Connection Between Intermittent Turbulent Activity Near the Wall of a Turbulent Boundary Layer with Pressure Fluctuations at the Wall," M.I.T. Acoustics and Vibration Laboratory report No. 70208-10.

Burke, S.E. 1984 MIT Acoustics and Vibration Laboratory, personal communication.

Coles, D.E. 1968 "Computation of Turbulent Boundary Layers," 1968 AFOSR-IFP-Stanford University Conference Proceedings, vol. 2, Stanford Univ., pp. 1-45.

Cook, N.H., & Rabinowicz, E. 1963 Physical Measurement and Analysis, Addison-Wesley, Reading, MA.

Crandall, S.H., Karnopp, D.C., Kurtz, E.F., Jr., & Pridmore-Brown, D.C. 1968 Dynamics of Mechanical and Electromechanical Systems, McGraw-Hill, New York.

Crandall, S.H., & Mark, W.D. 1973 Random Vibration in Mechanical Systems, Academic Press, New York.

Crandall, S.H., Dahl, N.C., & Lardner, T.J. 1978 An Introduction to the Mechanics of Solids, 2nd ed., McGraw-Hill, New York.

Escudier, M.P., Bornstein, J., Acharya, M., & Vokurka, V. 1982 "Development of a Floating-Element for the Measurement of Surface Shear Stress," unpublished paper, Brown Boveri Research Centre, Baden (Switzerland), January 1982.

Frei, D., & Thomann, H. 1980 "Direct Measurements of Skin Friction in a Turbulent Boundary Layer with a Strong Adverse Pressure Gradient," Journal of Fluid Mechanics, vol. 101, part 1, pp. 79-95.

Froude, W. 1872 "Experiments on the Surface-Friction Experienced by a Plane Moving through the Water," reprinted in The Papers of William Froude, Institution of Naval Architects, London, 1955, pp. 138-146.

Gedney, C.J. 1979 "Wall Pressure Fluctuations During Transition on a Flat Plate," M.I.T. Acoustics and Vibration Laboratory report No. 84618-1.

Hanson, C.E. 1969 "The Design and Constructing of a Low-Noise, Low-Turbulence Wind Tunnel, M.I.T. Acoustics and Vibration Lab Report No. 79611-1.

Hudson, R.G. 1944 The Engineers' Manual, Wiley, New York.

Jung, W.G. 1980 IC Op-Amp Cookbook, Howard W. Sams and Co., Indianapolis.

Lancaster, D. 1982 Active-Filter Cookbook, Howard W. Sams and Co., Indianapolis.

Lueptow, R.M.	1984	MIT Acoustics and Vibration Laboratory, personal communication.
McMichael, J.M., Klebanoff, P.S., & Mease, N.E.	1979	"Experimental Investigation of Drag on a Compliant Surface," Progress in Astronautics and Aeronautics, vol. 72, pp. 410-438.
Moeller, M.J.	1983	"Measurement of Unsteady Forces on a Circular Cylinder in a Cross Flow at Subcritical Reynolds Numbers," Ph. D. thesis, MIT, Cambridge, MA.
Murlis, J., Tsai, H.M., & Bradshaw, P.	1982	"The Structure of Turbulent Boundary Layers at Low Reynolds Numbers," Journal of Fluid Mechanics, vol. 122, pp. 13-56.
Musker, A.J.	1979	"Explicit Expression for the Smooth Wall Velocity in a Turbulent Boundary Layer," AIAA Journal, vol. 17, no. 6, June 1979, pp. 655-657.
Nguyen, V.D., Dickenson, J., et. al.	1984	"Some Experimental Observations of the Law of the Wall Behind Large-Eddy Breakup Devices Using Servo-Controlled Skin Friction Balances," AIAA-84-0346.
Paros, J.M.	1970	"Application of the Force-Balance Principle to Pressure and Skin Friction Sensors," Proceedings of the Institute of Environmental Sciences, 1970, pp. 363-368.
Peterson, K.E.	1982	"Silicon as a Mechanical Material," Proceedings of the IEEE, vol. 70, no. 5, May 1982, pp. 420-457.
Schlichting, H.	1979	Boundary Layer Theory, 7th ed., trans. by J. Kestin, McGraw-Hill, New York.

Shapiro, P.J. 1977 "The Influence of Sound Upon Boundary Layer Instabilities," M.I.T. Acoustics and Vibration Laboratory Report No. 83458-83560.

Todd, F.H. 1967 "Resistance and Propulsion," Chapter VII in Principles of Naval Architecture, Society of Naval Architects & Marine Engineers, New York, pp. 288-462.

White, F.M. 1974 Viscous Fluid Flow, McGraw-Hill, New York.

Winter, K.G. 1977 "An Outline of the Techniques Available for the Measurement of Skin Friction in Turbulent Boundary Layers," Progress in the Aerospace Sciences, vol. 18, Pergamon Press, Great Britain, pp. 1-57.

APPENDIX A

CALCULATIONS

A.1 Transducer Model

A.2 Beam Element Equation of Motion

A.3 Transducer Response

A.4 Transducer Sensitivity to Inclination

A.1 Transducer Model

Using the model of Figure A.1, it is possible to develop a general theory to describe the output of the wall shear transducer with arbitrary input. Figure A.1 highlights the important facets of transducer operation:

- the wall shear stress causes a deflection of the beam element;
- deflection of the beam element alters its capacitance with respect to a stationary parallel plate;

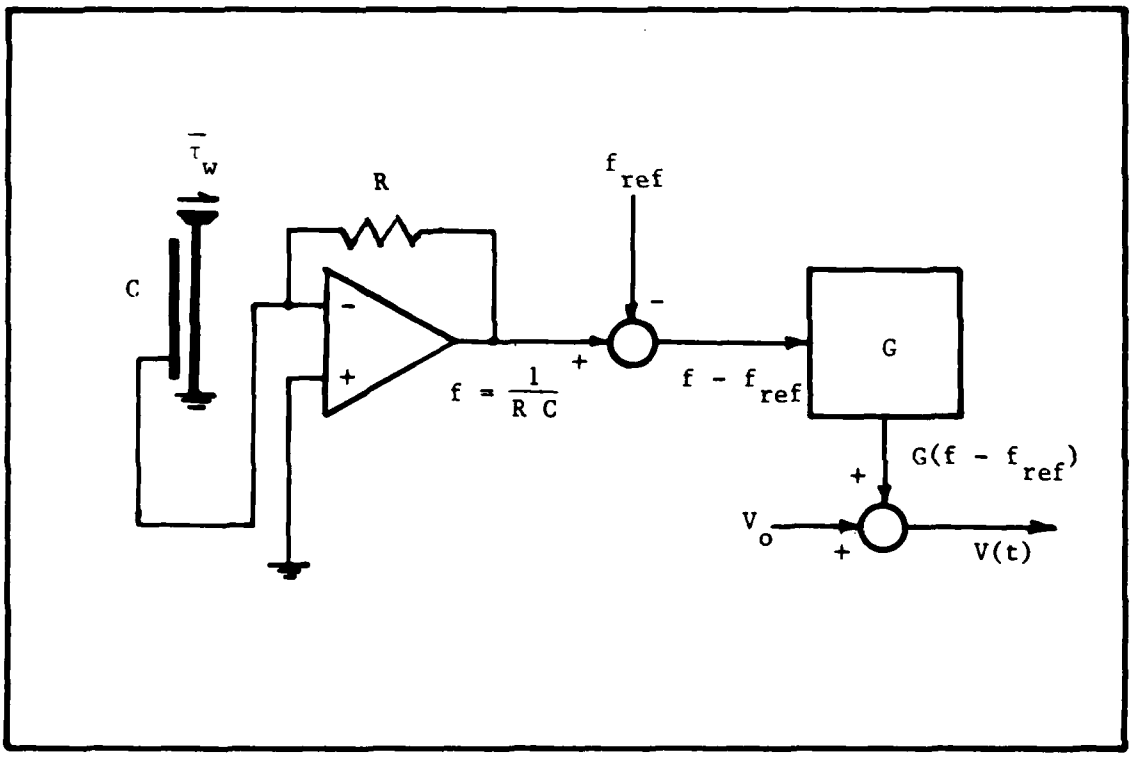

FIGURE A.1 Transducer Model

- the change in capacitance of the beam element-stationary plate changes the oscillation frequency f of an astable multivibrator, since the oscillation frequency is inversely proportional to the capacitance; and
- the frequency difference between the oscillator signal and a reference frequency f_{ref} is then converted to a voltage which is added to an offset voltage V_o, generating the transducer output.

The capacitance of a parallel plate capacitor is given by

$$C = K \frac{w\,L}{s} \qquad \left[\text{Hudson (1944)}\right] \tag{A1.1}$$

where K is a constant of proportionality, L is the length and w the width of each plate, and s is the distance between plates. If one plate is deflected a small transverse amount, then the distance s is no longer constant but rather a function of x, the coordinate along the undeflected length of the movable plate measured from the wall. Further, the deflection may also be a function of time. Effectively, s not a constant leads to an infinite number of parallel capacitances

$$dC = K \frac{w}{s(x,t)}\,dx \tag{A1.2}$$

in the limit of small plate deflections. If now s(x,t) is de-

fined as

$$s(x,t) \equiv d_o + y(x,t) \ , \tag{A1.3}$$

where d_o is the undeflected capacitor plate spacing and $y(x,t)$ is the transverse deflection of the movable plate, then

$$dC = K \frac{w}{d_o + y(x,t)} dx = K \frac{w\,L}{d_o} \frac{d\left(\frac{x}{L}\right)}{1 + \frac{y(x,t)}{d_o}} \ . \tag{A1.4}$$

Nondimensionalizing and defining

$$\frac{x}{L} \equiv \xi \qquad\qquad \frac{y}{d_o} \equiv \eta(\xi,t) \tag{A1.5}$$

and noting that

$$K \frac{w\,L}{d_o} \equiv C_o \ , \tag{A1.6}$$

where C_o is the capacitance of the stationary-movable plate pair with the movable plate undeflected, equation A1.4 becomes

$$dC = C_o \frac{d\xi}{1 + \eta(\xi,t)} \ . \tag{A1.7}$$

Equation A1.7 is valid only for small deflections $\eta(\xi,t)$, for which three dimensional effects are insignificant. The total capacitance may be found to be

$$C = \int dC = C_o \int_0^1 \frac{d\xi}{1 + \eta(\xi,t)} , \qquad \text{(A1.8)}$$

"summing" over all the infinitesmal capacitances dC.

The oscillation frequency of the astable multivibrator is given by

$$f = \frac{1}{R\,C} \qquad \text{(A1.9)}$$

where C is the capacitance of the transducer and R is a feedback resistance (constant). Then, for a deflection of the movable plate $\eta(\xi,t)$, the oscillator frequency is

$$f = \frac{1}{R\,C} = \frac{1}{RC_o} \frac{1}{\int_0^1 \frac{d\xi}{1 + \eta(\xi,t)}} \qquad \text{(A1.10)}$$

or

$$f = f_o \frac{1}{\int_0^1 \frac{d\xi}{1 + \eta(\xi,t)}} \qquad \text{(A1.11)}$$

Since

$$V(t) = V_o + G\,(\,f - f_{ref}\,) \qquad \text{(A1.12)}$$

it is appropriate to select $f_{ref} = f_o$ to obtain

$$V(t) = V_o + G\, f_o \left(\frac{f}{f_o}\right) - 1 \qquad \text{(A1.13)}$$

or

$$V(t) = V_o + G\, f_o \quad \frac{1}{\int_0^1 \frac{d\xi}{1 + \eta(\xi,t)}} \qquad \text{(A1.14)}$$

using equation A1.11.

The normalized transducer output is given by

$$\frac{V(t) - V_o}{G\, f_o} = \frac{1}{\int_0^1 \frac{d\xi}{1 + \eta(\xi,t)}} - 1 \,. \qquad \text{(A1.15)}$$

The deflection $\eta(\xi,t)$ is determined by the transducer's excitation and dynamics considered in the following section.

A.2 Equation of Motion

The dynamics of the movable plate of the transducer determines how the transducer will respond to applied loads. The movable plate is cantilevered at its base and has a floating element mounted on its free end. The movable plate and floating element, together called the beam element, may be modeled as in Figure A.2.

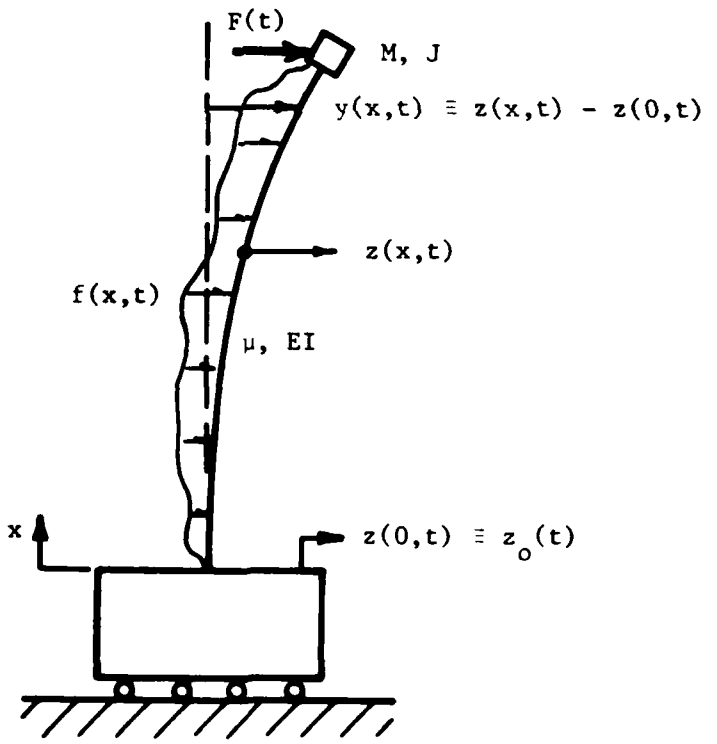

FIGURE A.2 Beam Element Dynamic Model

The floating element is modeled as a mass M and mass moment of inertia J lumped at the free end of the cantilever plate, modeled as a uniform beam of flexural rigidity EI and mass per unit length μ. The motion of the beam element is described by $z(x,t)$ in a stationary reference frame. In order to develop the equations of motion for general excitation, a concentrated transverse force $F(t)$ is applied to the floating element and a distributed transverse force $f(x,t)$ is applied along the beam.

Of interest in the current situation is the motion of the beam element relative to its base rather than its absolute motion $z(x,t)$, since the stationary capacitor plate is actually fixed with respect to the cantilever's base. In effect, it is desired to obtain the equations of beam element motion in the non-inertial reference frame translating with the cantilever's base.

If

$$z_o(t) \equiv z(0,t) \tag{A2.1}$$

is the translation of the base of the beam element, then the relative motion of the beam with respect to its base is

$$y(x,t) \equiv z(x,t) - z_o(t). \tag{A2.2}$$

Using the variational technique [Crandall, et. al. (1968)] and assuming small deflections of the beam, the equation of motion of the beam element is obtained as

$$\mu \frac{\partial^2 y}{\partial t^2} + EI \frac{\partial^4 y}{\partial t^4} + \mu \frac{d^2 z_o}{dt^2} = f(x,t) \tag{A2.3}$$

subject to the boundary conditions

$$\left.\begin{aligned} &\delta y \left[EI \frac{\partial^3 y}{\partial x^3}\right] = 0 && \text{(A2.4a)} \\ &\delta \left(\frac{\partial y}{\partial x}\right)\left[EI \frac{\partial^2 y}{\partial x^2}\right] = 0 && \text{(A2.4b)} \end{aligned}\right\} \quad x = 0$$

$$\left.\begin{aligned} &\delta y \left[- M \frac{\partial^2 y}{\partial t^2} + \frac{d^2 z_o}{dt^2} + EI \frac{\partial^3 y}{\partial x^3} + F(t)\right] = 0 && \text{(A2.4c)} \\ &\delta \left(\frac{\partial y}{\partial x}\right)\left[- J \frac{\partial^3 y}{\partial t^2 \partial x} - EI \frac{\partial^2 y}{\partial x^2}\right] = 0 && \text{(A2.4d)} \end{aligned}\right\} \quad x = L$$

where δ is the variational operator. For the case where the beam is cantilevered at its base,

$$\delta y \Big|_{x=0} \equiv \delta \left(\frac{\partial y}{\partial x}\right) \Big|_{x=0} \equiv 0 \tag{A2.5}$$

so that boundary conditions A2.4a and b are identically satisfied.

Clamped-Free Beam.

In the case of normal transducer operation, the beam element is free at x=L so that the variations in y and $\frac{\partial y}{\partial x}$ at x=L do not vanish identically, requiring the terms in brackets in equations A2.4c and d to be equal to zero. Thus,

$$\mu \frac{\partial^2 y}{\partial t^2} + EI \frac{\partial^4 y}{\partial t^4} = f(x,t) - \mu \frac{d^2 z_o}{dt^2} \qquad \text{(A2.6)}$$

with boundary conditions

$$y(0,t) \equiv 0 \qquad \text{(A2.7a)}$$

$$\frac{\partial y}{\partial x}(0,t) \equiv 0 \qquad \text{(A2.7b)}$$

$$M \frac{\partial^2 y}{\partial t^2}(L,t) - EI \frac{\partial^3 y}{\partial x^3}(L,t) = F(t) - M \frac{d^2 z_o}{dt^2} \qquad \text{(A2.7c)}$$

$$- EI \frac{\partial^2 y}{\partial x^2}(L,t) = J \frac{\partial^3 y}{\partial t^2 \partial x}(L,t) . \qquad \text{(A2.7d)}$$

Note that acceleration of the transducer base introduces D'Alembert or inertial force excitations proportional to $-\frac{d^2 z_o}{dt^2}$ in the field equation (A2.6) and the force boundary condition (A2.7c). If the transducer base is non-accelerating ($\frac{d^2 z_o}{dt^2} \equiv 0$), the transducer is kept vertical so that $f(x,t) \equiv 0$, and the floating element is properly aligned so that there are no error forces on the floating element ($F(t) \equiv \bar{\tau}_w(t) A_e$), then the field equation becomes

$$\mu \frac{\partial^2 y}{\partial t^2} + EI \frac{\partial^4 y}{\partial x^4} = 0 \qquad \text{(A2.8)}$$

subject to the revised boundary condition (A2.7c)

$$M \frac{\partial^2 y(L,t)}{\partial t^2} - EI \frac{\partial^3 y(L,t)}{\partial x^3} = \bar{\tau}_w(t)\, A_e \qquad \text{(A2.9)}$$

with the other three boundary conditions unchanged. Therefore, in the absence of the error terms specified above, the wall shear stress excites the homogeneous response of the beam $y(x,t)$ through the force boundary condition, equation A2.9. Transverse acceleration of the transducer base introduces not only a D'Alembert force at the floating element ($x=L$) equal to $-M \frac{d^2 z_o}{dt^2}$, but also a distributed D'Alembert force $-\mu \frac{d^2 z_o}{dt^2}$ along the length of the beam. Thus, the response of the beam element to transverse acceleration of its base is dynamically analogous to its response to the wall shear stress except that transverse acceleration gives rise to the aforementioned distributed D'Alembert force.

Clamped-Pinned Beam.

If the beam element is pinned at the floating element, then $\delta y \equiv 0$ at x=L and the equations describing the motion of the beam element are

$$\mu \frac{\partial^2 y}{\partial t^2} + EI \frac{\partial^4 y}{\partial x^4} = f(x,t) - \mu \frac{d^2 z_o}{dt^2} \qquad \text{(A2.6)}$$

with boundary conditions

$$y(0,t) \equiv 0 \qquad \text{(A2.7a)}$$

$$\frac{\partial y(0,t)}{\partial x} \equiv 0 \qquad \text{(A2.7b)}$$

$$y(L,t) \equiv 0 \qquad \text{(A2.10)}$$

$$- EI \frac{\partial^2 y(L,t)}{\partial x^2} = J \frac{\partial^3 y(L,t)}{\partial t^2 \partial x} . \qquad \text{(A2.7d)}$$

Because F(t) does not excite the transducer, the wall shear stress cannot either. Thus, if the floating element exhibits a pinned end condition, the beam element will not respond to the wall shear stress although it will respond to the tranverse acceleration of the transducer base (equation A2.6 applies).

Clamped-Clamped Beam.

If the floating element exhibits a clamped end condition, then equation A2.6 is still the appropriate field equation, with y and $\frac{\partial y}{\partial x}$ identically zero at x=0 and x=L. Again, the beam element will not respond to the wall shear stress but will respond to transverse acceleration of the transducer base.

A.3 Transducer Response

For frequencies much smaller than the fundamental resonant frequency of the beam element, the deflection shape of the beam element is satisfactorily described by its static deflection shape. Assuming that the transducer base is non-accelerating, that the transducer is kept vertical, and that there are no error forces on the floating element, equation A2.8 may be solved with equations A2.7a,b, and c and equation A2.9 for the static deflection shape (which is not a function of time). Assuming

$$F(t) = A_e \bar{\tau}_w(t) \tag{A3.1}$$

leads to

$$\eta(\xi,t) = \frac{A_e}{2 k_s d_o} (3\xi^2 - \xi^3) \bar{\tau}_w(t) \tag{A3.2}$$

where $k_s = 3EI/L^3$ is the effective stiffness of the beam in resisting an applied transverse force at the free end. alternatively, since

$$\epsilon(t) = \frac{A_e}{k_s} \bar{\tau}_w(t) \tag{A3.3}$$

is the transverse deflection of the free end of the beam,

$$\eta(\xi,t) = \frac{1}{2\,d_o}\,(3\xi^2 - \xi^3)\,\varepsilon(t) \qquad \text{(A3.4)}$$

describes the deflection shape of the beam element. Since

$$\frac{V(t) - V_o}{G\,f_o} = \frac{1}{\int_0^1 \frac{d\xi}{1 + \eta(\xi,t)}} - 1 \,, \qquad \text{(A1.15)}$$

it is possible to evaluate the transducer output as a function of $\overline{\tau}_w(t)$.

A.3.1 Linearized Response

If $\left|\eta(\xi,t)\right| << 1$, then

$$\frac{1}{\int_0^1 \frac{d\xi}{1 + \eta(\xi,t)}} \simeq \frac{1}{1 - \int_0^1 \eta(\xi,t)\,d\xi} \simeq 1 + \int_0^1 \eta(\xi,t)\,d\xi \,. \qquad \text{(A3.5)}$$

Thus,

$$\frac{V(t) - V_o}{G\,f_o} \simeq \int_0^1 \eta(\xi,t)\,d\xi \qquad \text{(A3.6)}$$

from which, with equation A3.2,

$$\frac{V(t) - V_o}{G\,f_o} \simeq \frac{A_e\,\overline{\tau}_w(t)}{2\,k_s\,d_o} \int_0^1 (3\xi^2 - \xi^3)\,d\xi \,. \qquad \text{(A3.7)}$$

Upon integration, equation A3.7 leads to

$$\frac{V(t) - V_o}{G f_o} \simeq \frac{3 A_e}{2 k_s d_o} \bar{\tau}_w(t) \qquad \text{(A3.8)}$$

which is shown in Figure 2.5 as a function of

$$\frac{\varepsilon}{d_o} = \frac{A_e \bar{\tau}_w}{k_s d_o} , \qquad \text{(A3.9)}$$

the normalized end deflection of the beam.

A.3.2 Exact Response

Using equation A3.4, the integral in equation A1.15 can be computed numerically for different $\frac{\varepsilon}{d_o}$. The results of this integration are shown in Figure 2.5.

A.4 Sensitivity to Inclination

When the transducer is inclined from the vertical by an angle θ_o, the beam element deflects by its own weight. For small inclinations from the vertical, the transverse component

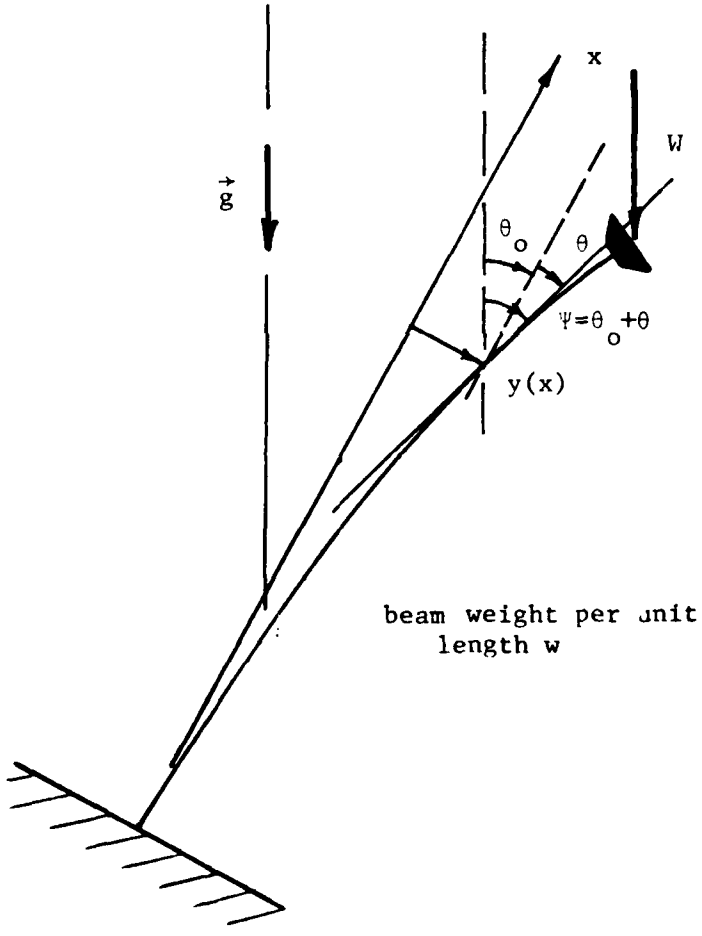

FIGURE A.3 Transducer Inclination Geometry

F_t of a load F is given by

$$F_t = F \sin \psi \simeq F \psi \ , \qquad \text{(A4.1)}$$

where ψ is the local angle between the tangent to the beam and the vertical shown in Figure A.3. Now,

$$\psi = \theta_o + \theta = \theta_o + \frac{dy}{dx} \qquad \text{(A4.2)}$$

where $\theta = \frac{dy}{dx}$ is the local angle between the tangent to the beam and the undeflected beam position and θ_o is the angle the transducer base is inclined from the vertical.

The beam element consists of a floating element of mass M and a cantilever plate of mass per unit length μ. In a gravity field, these possess weights of W and w, respectively. If the transducer is inclined from the vertical with no shear stress applied to the floating element and without accelerating the base of the transducer transversely, then, from equations A2.6 and A2.7 and by considering only static deflections y(x) of the beam element,

$$EI \frac{d^4y}{dx^4} = f(x,t) \qquad \text{(A4.3)}$$

subject to the boundary conditions

$$y(0) \equiv 0 \tag{A4.4a}$$

$$\frac{dy(0)}{dx} \equiv 0 \tag{A4.4b}$$

$$-EI \frac{d^3y(L)}{dx^3} = F(t) \tag{A4.4c}$$

$$\frac{d^2y(L)}{dx^2} \equiv 0 \quad . \tag{A4.4d}$$

Both f(x,t) and F(t) are developed by the weight of the cantilever plate and the floating element according to equations A4.1 and A4.2:

$$f(x,t) = w \left(\theta_o + \frac{dy}{dx} \right) \tag{A4.5}$$

$$F(t) = W \left(\theta_o + \frac{dy}{dx} \right). \tag{A4.6}$$

Equations A4.3 through A4.6 are then solved to obtain

$$\eta(\xi) = \left\{ C_1 + C_2 \exp(\beta\xi) + \right.$$

$$\left. \exp\left(-\frac{\beta}{2}\xi\right) \left[C_3 \sin \frac{\sqrt{3}}{2} \beta\xi + C_4 \cos \frac{\sqrt{3}}{2} \beta\xi \right] - \xi \right\} \frac{\theta_o L}{d_o} \quad , \tag{A4.7}$$

where θ_o is in radians and $\beta^3 \equiv \frac{wL^3}{EI}$. The coefficients C_i were calculated using the FORTRAN program GRAV3, owing to the complexity of the algebra and in order to facilitate the ready calculation of deflection shapes for different transducer parameters. The transducer parameters used for the calculations are:

$L = 31$ mm,

$d_o = 375$ μm ,

$M = 76$ mg,

$\mu = 16$ g/m, and

$EI = 2.84 \times 10$ Nm^2

for which

$C_1 = 1.1568$

$C_2 = 0.9807$

$C_3 = 2.1674$

$C_4 = -2.1375$

and $\beta = 0.254314$.

APPENDIX B

TRANSDUCER NATURAL FREQUENCIES

B.1 Clamped-Free Beam

The homogeneous form of equations A2.6 and A2.7 may be solved in order to determine the natural vibration frequencies of the clamped-free beam element:

$$\mu \frac{\partial^2 y}{\partial t^2} + EI \frac{\partial^4 y}{\partial t^4} = 0 \qquad \text{(B1.1)}$$

subject to the boundary conditions

$$y(0,t) \equiv 0 \qquad \text{(B1.2a)}$$

$$\frac{\partial y(0,t)}{\partial x} \equiv 0 \qquad \text{(B1.2b)}$$

$$M \frac{\partial^2 y(L,t)}{\partial t^2} - EI \frac{\partial^3 y(L,t)}{\partial x^3} = 0 \qquad \text{(B1.2c)}$$

$$EI \frac{\partial^2 y(L,t)}{\partial x^2} + J \frac{\partial^3 y(L,t)}{\partial^2 t \partial x} = 0 \qquad \text{(B1.2d)}$$

Separating variables and assuming time harmonic behavior leads to

$$y(x,t) = X(x)\ T(t) \qquad \text{(B1.3)}$$

where

$$X(x) = C_1 \sinh \lambda x + C_2 \cosh \lambda x + C_3 \sin \lambda x + C_4 \cos \lambda x \quad \text{(B1.4a)}$$

and

$$T(t) = e^{-i\omega t} \quad \text{(B1.4b)}$$

with

$$\lambda^4 = \frac{\omega^2 \mu}{EI} . \quad \text{(B1.5)}$$

Imposing the boundary conditions (B1.2) obtains

$$\frac{\cosh \lambda L + \cos \lambda L - \gamma(\sinh \lambda L - \sin \lambda L)}{\sinh \lambda L - \sin \lambda L - \gamma(\cosh \lambda L - \cos \lambda L)} + \frac{M}{\mu} \lambda = 0 \quad \text{(B1.6a)}$$

where

$$\gamma \equiv \frac{\sinh \lambda L + \sin \lambda L - \frac{\omega^2 J}{\lambda EI}(\cosh \lambda L - \cos \lambda L)}{\cosh \lambda L + \cos \lambda L - \frac{\omega^2 J}{\lambda EI}(\sinh \lambda L + \sin \lambda L)} . \quad \text{(B1.6b)}$$

The roots of equations B1.6 determine the eigenvalues λ_i . The first three natural frequencies have been calculated and are tabulated in Table V. The effect of the floating element's mass moment of inertia was approximated by modeling the element as a slab 4 mm by 4 mm and 2 mm thick, and was found to be negligible for the first three vibration modes.

B.2. Clamped-Pinned Beam

The determination of the resonant frequencies of the clamped-pinned beam follows the procedure for the clamped-free beam except that equation B1.2c is replaced by

$$y(L,t) \equiv 0 \quad . \tag{B2.1}$$

The characteristic equation then becomes

$$\sinh \lambda L - \sin \lambda L - \gamma(\cosh \lambda L - \cos \lambda L) = 0 \tag{B2.2}$$

where γ is as given in equation B1.6b. The natural frequencies of the first three clamped-pinned modes is tabulated in Table V, both including and neglecting the effect of the rotational inertia of the floating element. Blevins' (1979) tabulation of the natural frequencies for the clamped- pinned beam are the same as the natural frequencies predicted from equation B2.2 above.

B.3 Clamped-Clamped Beam

For the clamped-clamped case, the mass moment of inertia no longer enters the problem since

$$\frac{\partial y}{\partial x}(L,t) \equiv 0 \qquad \text{(B3.1)}$$

is the new boundary condition that replaces equation B1.2d. The natural frequencies of the first three clamped-clamped modes are taken from Blevins (1979) and shown in Table V.

TABLE V

Summary of Beam Element Natural Frequencies

Clamped-Free Beam	f_1	f_2	f_3
J = 0	61.7	414.2	1202
J ≠ 0	61.7	411.2	1180
Δ%	0	0.7%	1.9%

Clamped-Pinned Beam	f_1	f_2	f_3
J = 0	340.6	1104	2303
J ≠ 0	339.4	1091	2246
Δ%	0.4%	1.1%	2.5%

Clamped-Clamped Beam	f_1	f_2	f_3
	494.2	1362	2671

Notes:

1. All frequencies are in Hz.
2. J ≠ 0 indicates J assumed to 1.267×10^{-4} mg m^2, modeling the floating element as a rectangular slab 4 mm x 4 mm x 2 mm.
3. The floating element mass M and (where appropriate) mass moment of inertia J are modeled as being lumped at the unclamped end of the beam element.
4. Clamped-clamped data and verification of clamped-pinned calculations are from Blevins (1979).

APPENDIX C

UNCERTAINTY ANALYSIS

From equation 2.1,

$$\tau_w \simeq \frac{8\, k_s\, d_o}{3\, A_e f_o G}\,(V - V_o). \tag{C.1}$$

It is shown in Cook and Rabinowicz (1963) that if

$$q = F(a_i) \tag{C.2}$$

where F is a function of n independent variables a_i, then the most probable mean square error e_q^2 in the quantity q is

$$e_q^2 \simeq \sum_{i=1}^{n} \left(\frac{\partial F}{\partial a_i}\right)^2 e_{a_i}^2 , \tag{C.3}$$

assuming the a_i are statistically independent. Each term e_ζ denotes the error or uncertainty in the quantity ζ. From equation C.3,

$$\varepsilon_\tau^2 \simeq \varepsilon_k^2 + \varepsilon_d^2 + \varepsilon_A^2 + \varepsilon_f^2 + \varepsilon_G^2 + \varepsilon_{V_o}^2 \left(\frac{V_o}{\tau_w s_\tau}\right)^2 \tag{C.4}$$

where $\varepsilon_i \equiv \frac{e_i}{a_i}$ and the uncertainty in V(t) has been neglected since it is an order of magnitude smaller than e_{V_o}.

Since $k_s = 3EI/L^3 = \frac{3wt^3}{4L^3}$ and $A = w_e^2$, equation C.3 obtains

$$\varepsilon^2 \simeq \varepsilon_E^2 + \varepsilon_w^2 + (3\varepsilon_t)^2 + (3\varepsilon_L)^2 \tag{C.5a}$$

$$\simeq (.05)^2 + (.05)^2 + 9(.01)^2 + 9(.05)^2 \simeq .0284 \tag{C.5b}$$

and

$$\varepsilon_A^2 = 2\varepsilon_1^2 = 2(.05)^2 = 0.0050 \tag{C.6}$$

so that, from equation C.4,

$$\varepsilon_\tau^2 \simeq 0.0284 + (.05)^2 + 0.005 + (.01)^2 + (.05)^2 + (.10)^2\left(\frac{2.5\ \text{V}}{(1\ \text{Pa})(.4\ \text{V/Pa})}\right)^2 \simeq 0.429 \tag{C.7}$$

and

$$\varepsilon_\tau \simeq 0.66 \tag{C.8}$$